Chapter 5

PHOTOCHEMICAL HEME REDUCTION AND GAS BINDING IN CYTOCHROME P450

5.1. Background: reductive activation of dioxygen

The cytochrome P450 superfamily of heme enzymes catalyzes a wide variety of biologically important transformations, including the metabolism of fatty acids and biosynthesis of signaling molecules. As described in Chapter 1, one-electron reduction of the ferric heme active site induces binding of dioxygen; a second reduction, followed by protonation and heterolysis of the O–O bond generates the catalytically active species, compound I (CI, **Figure 5.1**). Natively, the electrons originate from reduced nicotinamide adenine dinucleotide (phosphate), NAD(P)H, and are passed to the heme by a series electron transfer (ET) partner proteins. However, these native ET steps are much slower than the reaction of CI with substrate.[1–3]

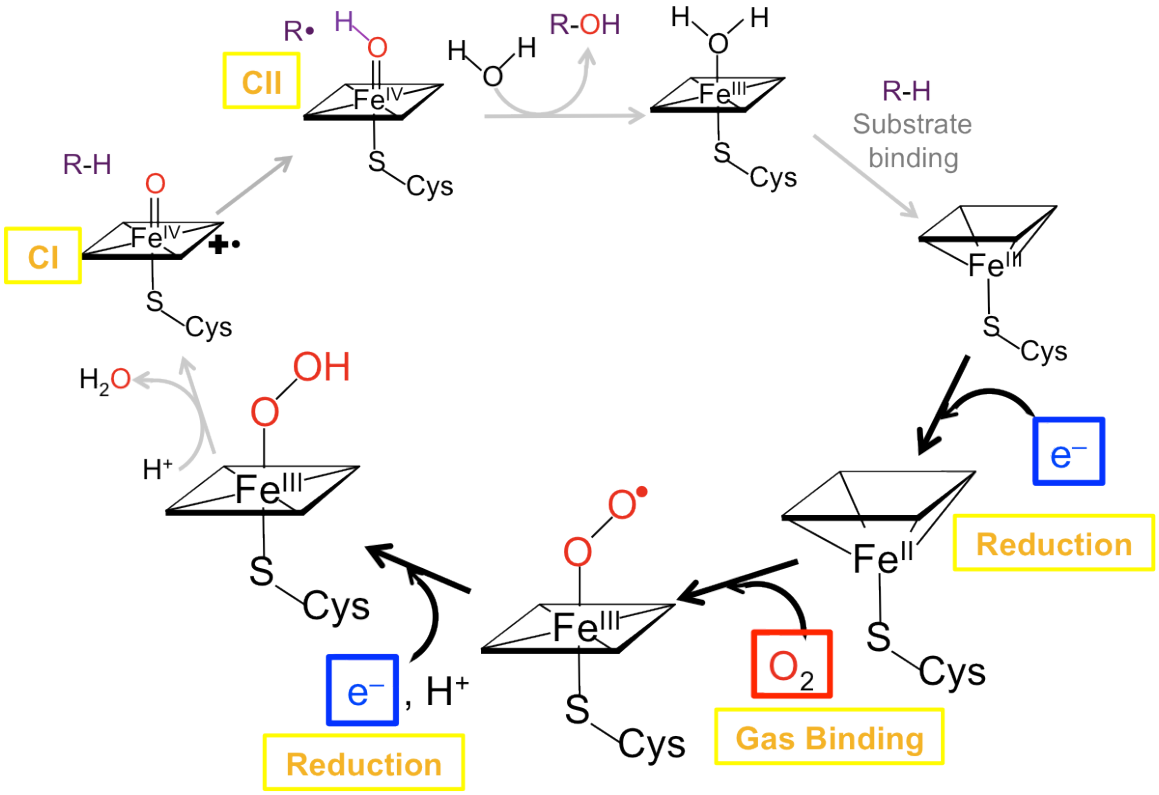

Figure 5.1. Canonical P450 catalytic scheme, highlighting the reductive ET events that activate dioxygen.

Many methods have been implemented in an effort to artificially generate and study this active species. Chemical oxidation by rapid mixing with peroxyacids such as *meta*-chloro-peroxybenzoic acid (*m*CPBA) was used to generate CI in highly purified samples of CYP119.[2] This method was successful for achieving spectroscopic characterization of the reactive intermediate, as well as single-turnover kinetics investigation of the reaction with substrate. However, the events of hydrogen abstraction to generate compound II (CII, **Figure 5.1**), and radical rebound to form hydroxylated substrate have yet to be observed directly. The dead-time of mixing experiments (e.g., 0.25-5 ms for Bio-Logic® SFM-400) preclude observation of reaction events that include hydrogen abstraction from substrate to form CII, and radical recombination which produces hydroxylated substrate.

In Chapter 2, we described how covalent tethering of a ruthenium photosensitizer to the P450 surface (**Figure 5.2**) can be used to photochemically generate the catalytically-relevant one-electron oxidized species, CII. The deadtime for monitoring these photo-triggered events is limited only by the laser pulse-width (~8 ns in the systems employed for these studies) and instrument response (< 30 ns). We were able to observe CII formation on the low millisecond timescale; this is at least two orders of magnitude faster than expected production by a chemical mixing reaction.

However, this photochemical method has significant limitations. The yields of oxidized products are low (estimated at < 20%). Additionally, each laser pulse can only initiate a single ET event; two oxidizing equivalents are needed to generate CI. Furthermore, photochemical heme oxidation proceeds at low driving force, and is sensitive to the intervening medium (see Chapters 3 and 4). Efforts to

reproduce this ET reactivity in the thermophilic CYP119 generated CII with even lower yield (< 5%).

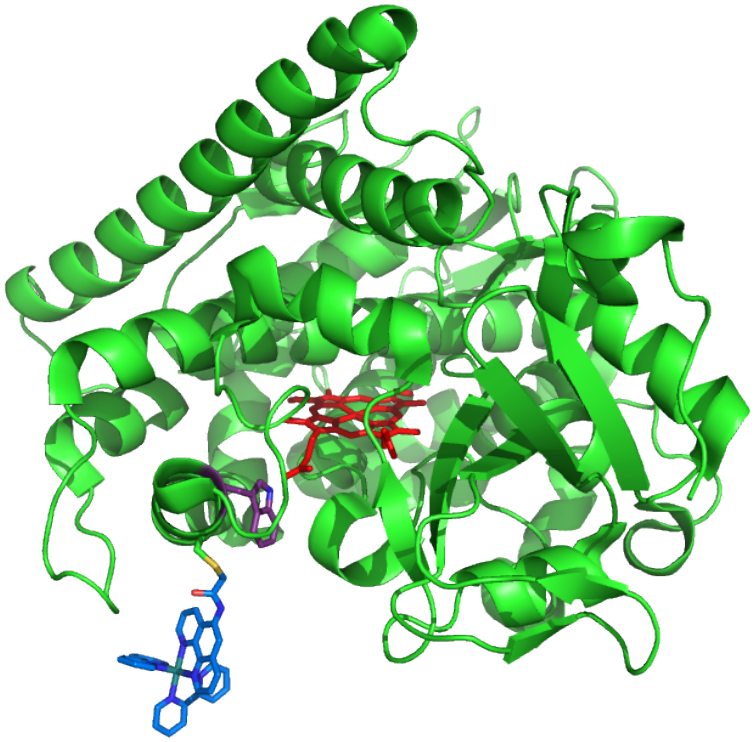

Figure 5.2. Structure of the Ru-P450$_{BM3}$ conjugate. (PDB: 3NPL)

As described in Chapter 1, many features of the cytochrome P450 structure have evolved to facilitate enzyme reduction and the activation of dioxygen - not oxidative ET and activation of water. By using our tethered photosensitizer as a replacement for the native ET partners, we anticipated that *reductive* flash-quench (**Figure 5.3**) could be used to study other important aspects of the catalytic cycle, and may even be used to rapidly access CI.

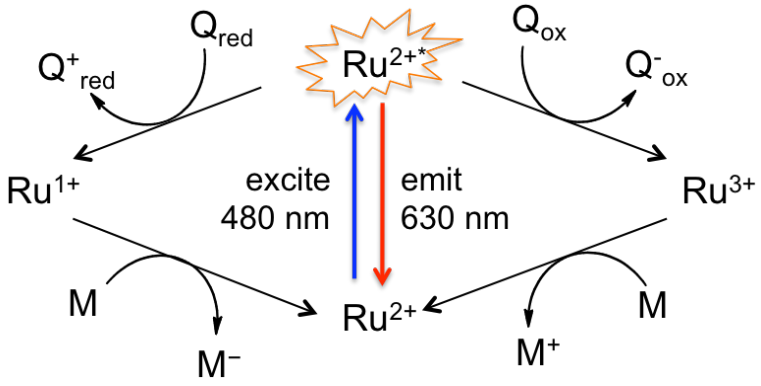

Figure 5.3. Flash-quench cycles for ET with the heme active site.

By supplying an appropriate small molecule quencher such as *para*-methoxydimethylaniline (*p*MeODMA), we can photochemically generate a reduced photosensitizer (Ru^{1+}, best characterized as $Ru^{II}bpy^{\bullet-}$). This species has almost 1 eV of driving force for reduction of the P450 heme: $E°(Ru^{II}bpy/Ru^{II}bpy^{\bullet-})$ = –1.3 V vs. NHE;[4,5] $E°$(P450 $Fe^{III/II}$) = –0.43 V vs. NHE.[6] These flash quench methods have been used to photochemically reduce Ru-labeled cytochrome *c*.[7] They also were used to reduce Ru-labeled cytochrome P450-BM3 at residue 387, however, conjugation of the photosensitizer at residue 62 curiously showed no heme reduction.[8]

We set out to examine each successive step of P450 oxygen activation by photo-triggered methods, using tethered Ru photosensitizers as the source for reductive ET. We examine photochemical heme reduction, the first step in catalysis. We anticipated that this phototriggered method also could be used to initiate the second step in the native P450 catalytic cycle: binding of dioxygen to the active site. The binding of dioxygen to ferrous heme results in formation of a ferric-superoxo; this species is not thermally stable at room temperature, and decomposes to release superoxide (auto-oxidation).[9] Carbon monoxide is often used as a more stable diatomic analogue. In some P450 variants, the Fe^{II}-CO species undergoes protonation and/or dissociation of the proximal cysteine

thiolate ligand to generate an inactive species known as "P420."[10–12] In our hands, the ferrous-CO complex of CYP119 is stable for up to seven months at 4 °C with no apparent change to the UV-visible absorbance spectrum. This approach of photo-triggering heme reduction and observing gas binding has been implemented by others, using organic photosensitizers; UV excitation of NADH was used to trigger P450 reduction via the NADH triplet excited state, and the authors observed binding of CO.[13]

The rate of CO binding to heme enzymes also can be examined by photolysis and *re*binding. Excitation into the Fe^{II}–CO Soret or Q-bands causes nearly instantaneous photolysis and dissociation of CO. Some portion of the dissociated CO is remains trapped within the protein pocket and rebinds rapidly to the five-coordinate ferrous heme – this is known as geminate recombination.[14–16] Another portion of the dissociated CO has sufficient energy to escape into solution, and thus takes significantly longer to re-enter the protein cavity and rebind to the heme. Photolysis has been used to measure the rates of rebinding for both P450 BM3,[15,16] and CYP119[17]. However, in the latter case of thermophlic CYP119, only room temperature rebinding has been reported, and sub-nanosecond kinetics have not been examined.

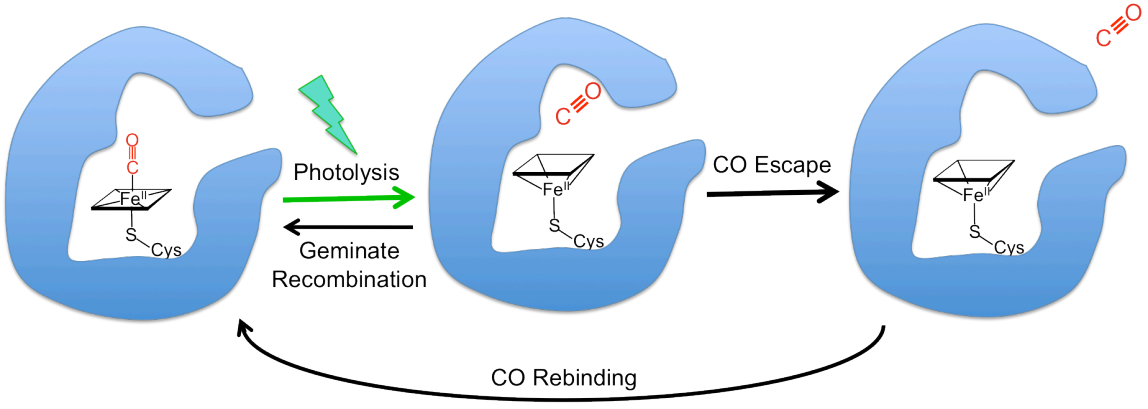

Figure 5.4. Cartoon of CO photolysis and rebinding. The blue shape represents the protein framework.

The third step in P450 catalysis involves a second ET event to produce the ferric superoxo; this final species converts directly to CI. This second electron also could be supplied by flash-quench. However, as addressed in Chapter 3, the yields and lifetimes of flash-quench generation of intermediates precludes the use of two sequential flash-quench cycles. It would be more effective to chemically generate a semi-stable pool of $Fe^{III}–O_2^{\bullet-}$. A stable ferric superoxo can be generated for the substrate bound P450 BM3 at low temperature (-60 °C) in Tris buffer.[18] At these temperatures, the cryosolvent of 70:30 glycerol:Tris buffer behaves as a semi-solid glass, which would greatly inhibit bimolecular quenching reactions. There may be a higher temperature at which the $Fe^{III}–O_2^{\bullet-}$ lifetime is sufficiently long; one minute or more would allow flash-quench ET to generate $Fe^{III}–O_2^{2-}$, and observe the conversion to CI.

Another significant challenge facing flash-quench reduction of $Fe^{III}–O_2^{\bullet-}$ is that the ruthenium metal-to-ligand charge transfer (MLCT) bands overlap significantly with the P450 Soret and Q-bands; excitation into these protein absorptions can cause photodissociation of O_2, analogous to $Fe^{II}–CO$. If the yields of photodissociation are competitive with yields of ruthenium excited state, it will be difficult or impossible to observe reduction of $Fe^{III}–O_2^{\bullet-}$ to $Fe^{III}–O_2^{2-}$ and subsequent formation of CI.

In this Chapter, we examine the kinetics of flash-quench heme reduction and assess the possibility for monitoring photochemical reduction-triggered gas binding. We then examine the kinetics of photo-triggered CO dissociation and re-binding to the heme for the thermophilic CYP119 under varying conditions of laser power, temperature, and the presence or absence of substrate. We identify unique aspects of CYP119 conformational dynamics, and assess thermodynamic activation parameters for the rebinding process.

5.2. Results and Analysis

5.2.1. Reductive flash-quench

We examined the photochemical reduction of four Ru-P450 conjugates that are described in Chapter 3: two are mutants of P450 BM3 from *Bacillus megaterium* (Ru_{C97}-BM3(W_{96}), Ru_{C97}-BM3($_{W}H_{96}$)) and two are mutants of CYP119, the thermophilic P450 from *Sulfolobus acidocaldarius* (Ru_{C77}-CYP119(H_{76}), Ru_{C77}-CYP119($_{H}W_{76}$)). Subscripts after Ru indicate the tethering location, i.e., non-native cysteine 97 or 77; subscripts in parentheses indicate the native residue. The presence of tryptophan directly adjacent to the tethering point (W96 or W76, for P450 BM3 and CYP119, respectively) was found to facilitate photochemical heme oxidation by acting as a redox intermediate for multistep hole transfer. However, we did not anticipate that these residues can participate in multistep *reductive* ET.

Luminescence

As described in Chapters 2 and 3, excitation at 480 nm results in luminescence (λ_{max} = 630 nm) of both the free photosensitizer ([Ru(2,2′-bipyridine)$_2$(5-acetamido-1,10-phenanthroline)]$^{2+}$, abbreviated [Ru(bpy)$_2$(Aphen)]$^{2+}$) and the Ru-P450 conjugates. The photosensitizer has a monoexponential luminescence decay rate of 720 ns in deoxygenated buffer (50 mM sodium borate, pH 8). All of the Ru-P450 conjugates display biexponential luminescence decays; we attribute this observation to multiple conformations of the photosensitizer, which do not exchange on the timescale of this measurement. In the presence of 10 mM *p*MeODMA, luminescence lifetimes are significantly quenched (**Figure 5.5**), and can be fit to a monoexponential decay. Unlike what was observed for oxidative quenching with [Ru(NH$_3$)$_6$]$^{3+}$ in Chapter 3, there is very little difference in the quenched lifetimes among the different Ru-P450 conjugates (**Table 5.1**).

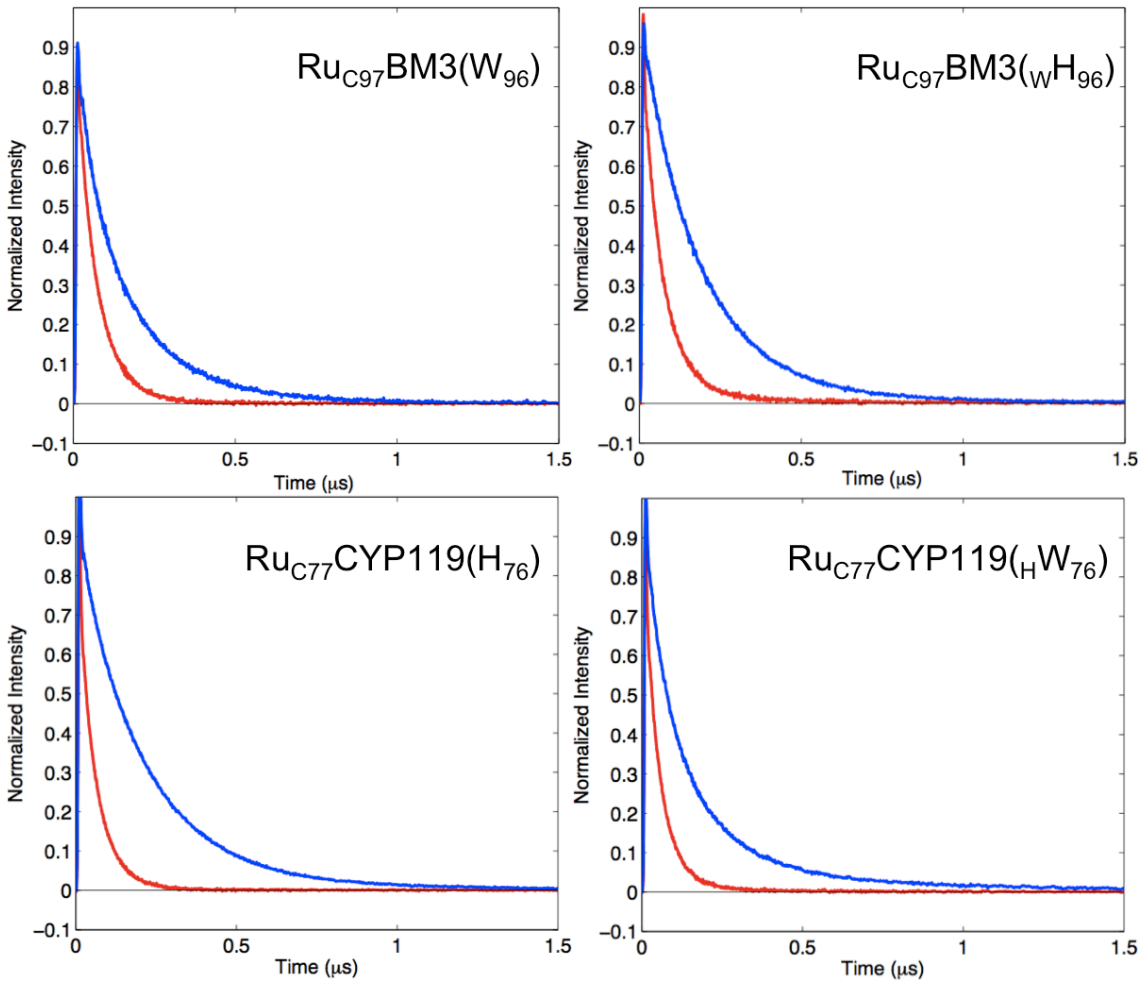

Figure 5.5. Luminescence decay at 630 nm of four Ru-P450 conjugates in the presence and absence of *p*MeODMA. λ(excitation) = 480 nm.

Table 5.1. Luminescence lifetimes, taken from biexponential (unquenched) and monoexponential (quenched) fits.

Enzyme	conditions	τ_{mono}(ns)	τ_{a}(ns)	τ_{b}(ns)	%a	%b
Ru$_{C97}$-BM3(W$_{96}$)	unquenched		190	52	65	35
	*p*MeODMA	62				
Ru$_{C97}$-BM3($_{W}$H$_{96}$)	unquenched		160	310	80	20
	*p*MeODMA	65				
Ru$_{C77}$-CYP119(H$_{76}$)	unquenched		220	45	85	15
	*p*MeODMA	54				
Ru$_{C77}$-CYP119($_{H}$W$_{76}$)	unquenched		91	320	75	25
	*p*MeODMA	50				

Single-wavelength transient absorption

We have used single-wavelength transient absorption spectroscopy to monitor the flash-quench heme reduction in Ru-P450 systems. As described in Chapters 2 and 3, both the Ru photosensitizer and P450 heme have strong electronic absorbance in the 390-440 nm region (P450 Soret $\varepsilon(\lambda_{max}$: 418 nm) = 95,000 $M^{-1}cm^{-1}$;[1] $[Ru(bpy)_2(Aphen)]^{2+}$ $\varepsilon(\lambda_{max}$: 450 nm) = 16,600 $M^{-1}cm^{-1}$ [19]). The shapes and positions of these electronic transitions are sensitive to metal oxidation state and environment; and each species has a distinct absorption profile. By monitoring multiple wavelengths over time, we can identify the formation and decay of ET intermediates following laser excitation. This process is greatly facilitated by control studies (e.g., the absence of quencher), as well as comparison to absorption profiles in the literature.

In the absence of *p*MeODMA quencher, we observe transient bleaching ($\Delta OD<0$) in the 400-440 nm visible region that is due to bleaching of the Ru photosensitizer MLCT band (see Chapters 2 and 3 for experimental data). The wavelength profiles of these transients are essentially identical for the free photosensitizer and the Ru-P450 conjugates, and the features return to baseline with the same decay constant as the luminescence lifetimes.

The Ru-P450 conjugates display multiphasic TA kinetics in the presence of *p*MeODMA (**Figure 5.6**).

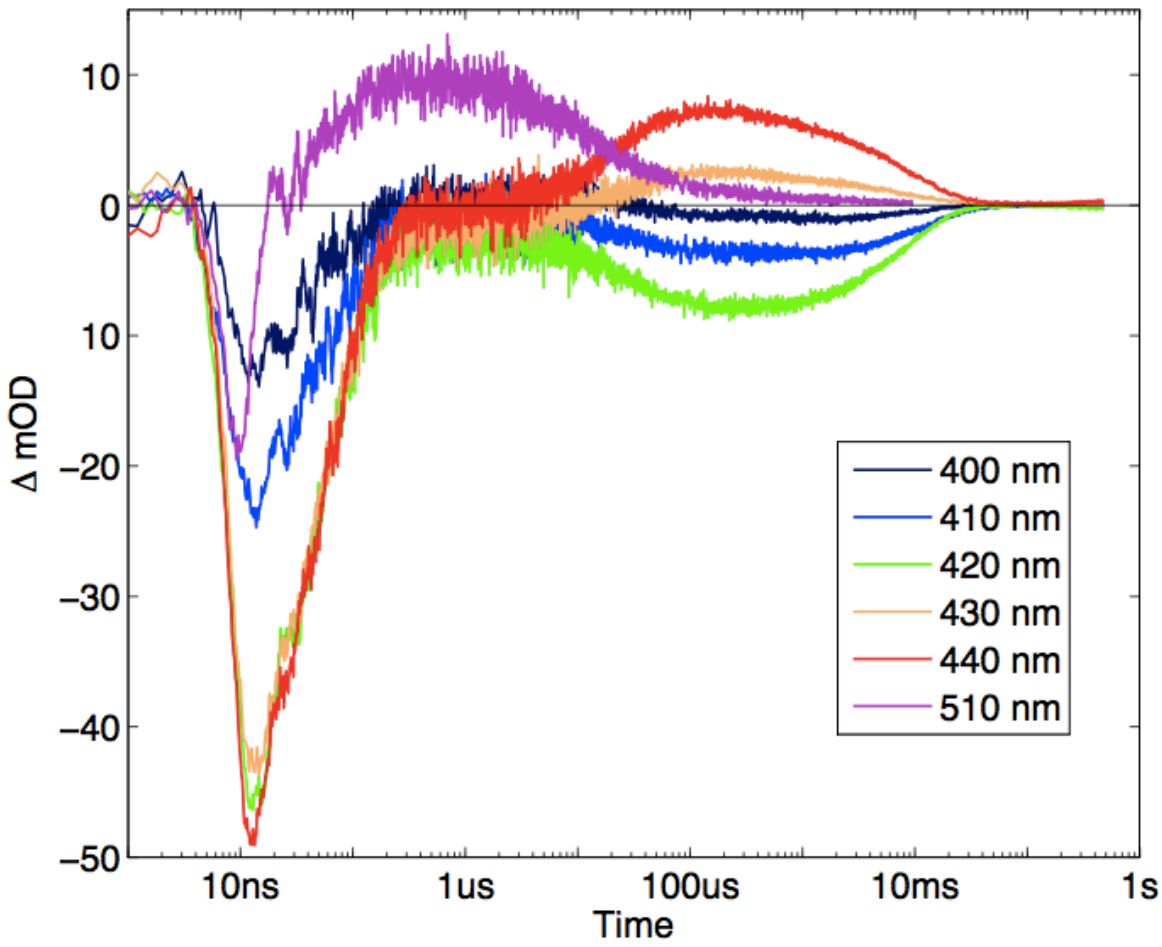

Figure 5.6. Single-wavelength transient absorption data of Ru-P450 at various wavelengths. Sample composition: 10 μM Ru_{C97}-BM3(W_{96}), 10 mM *p*MeODMA, 50 mM sodium borate, pH 8.

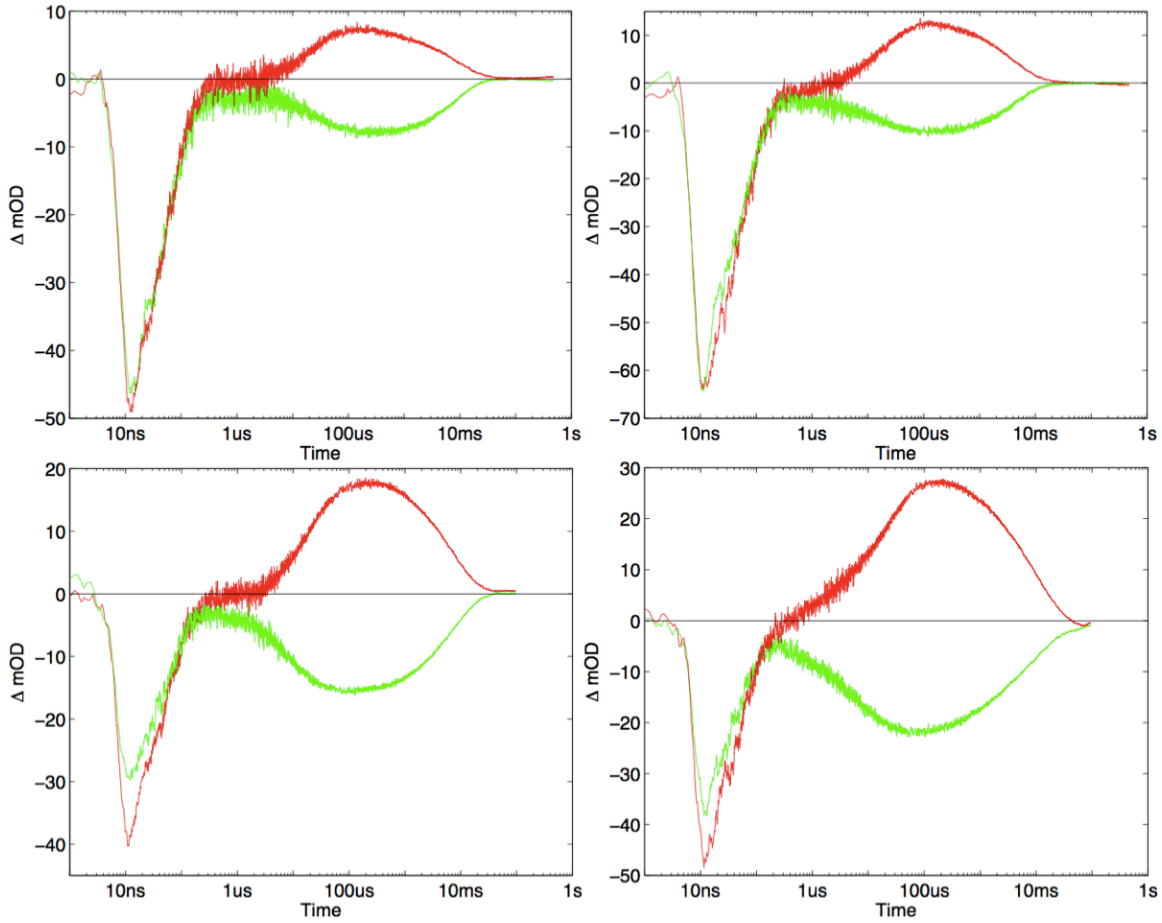

Figure 5.7. Single wavelength transient absorption data for flash-quench of four Ru-P450 mutants. $\lambda_{excitation}$ = 480 nm, λ_{probe} = 420 nm (green), 440 nm (red). Samples consisted of 10 μM Ru-P450, 10 mM *p*MeODMA, 50 mM sodium borate, pH 8. **Top left**: Ru_{C97}-BM3(W_{96}). **Top right**: Ru_{C97}-BM3($_{W}H_{96}$). **Bottom Left**: Ru_{C77}-CYP119(H_{76}). **Bottom Right**: Ru_{C77}-CYP119($_{H}W_{76}$)

Assignment of Intermediates

This first transient is assigned as the $^{*}Ru^{II}$ excited state, in analogy to control studies; this feature decays rapidly, with the same decay constant as the quenched luminescence lifetime. A transient absorption feature at 510 nm appears at this same rate, and decays on the microsecond-to-millisecond timescale. Quenching of the Ru excited state results in formation of a *p*MeODMA radical cation; this species has been characterized by transient absorption, with an absorbance maximum of 484 nm (ε(484)=7200 $M^{-1}cm^{-1}$).[20,21] This wavelength is too close to

the excitation wavelength to reliably probe, but there is still significant *p*MeODMA$^{\bullet+}$ absorbance at 510 nm, and we attribute our transient feature to this species.

Additionally, a new transient absorption feature appears on the microsecond timescale that is characterized by a bleach centered at 420 nm and a concomitant increase in absorption centered at 440 nm. TA at all wavelengths decay to baseline within the course of one second, indicating that the ET reaction is reversible.

It is of note that the red-shift associated with the observed transient species is different from the blue-shift and broadening associated with dithionite-induced heme reduction (**Figure 5.8**). The ferrous-ferric difference spectrum of WT P450 BM3 has maxima at 390, 460, and 550 nm, and a minimum at 420 nm; the transiently reduced spectrum has a maximum at 440 nm and minimum at 420 nm. This discrepancy also was observed for photochemical reduction of inducible nitric oxide synthase using non-covalently bound ruthenium wires.[22] The spectral differences were attributed to a difference in spin state and coordination; chemically-reduced P450 and NOS are five-coordinate and high-spin. However, the rate of photochemical reduction may exceed ligand-loss and spin-conversion, resulting in a transient, low-spin ferrous species. The TA features of photochemically-reduced Ru-P450 conjugates are consistent with that observed upon flash-quench reduction of cytochrome P450$_{cam}$ using imidazole-terminated Ru-photosensitizer wires that bind in the P450 substrate channel and ligate the heme iron (**Figure 5.8,** inset).[23] Cryoreduction of P450cam at 77 K similarly resulted in a low-spin six-coordinate ferrous species with absorption around 440 nm, which converted to five-coordinate, high-spin upon annealing at higher temperatures.[24] Thus, we assign the feature at ~100 μs to low-spin ferrous P450.

This reversibly reoxidizes to ferric on the millisecond timescale, and we observe no additional intermediates.

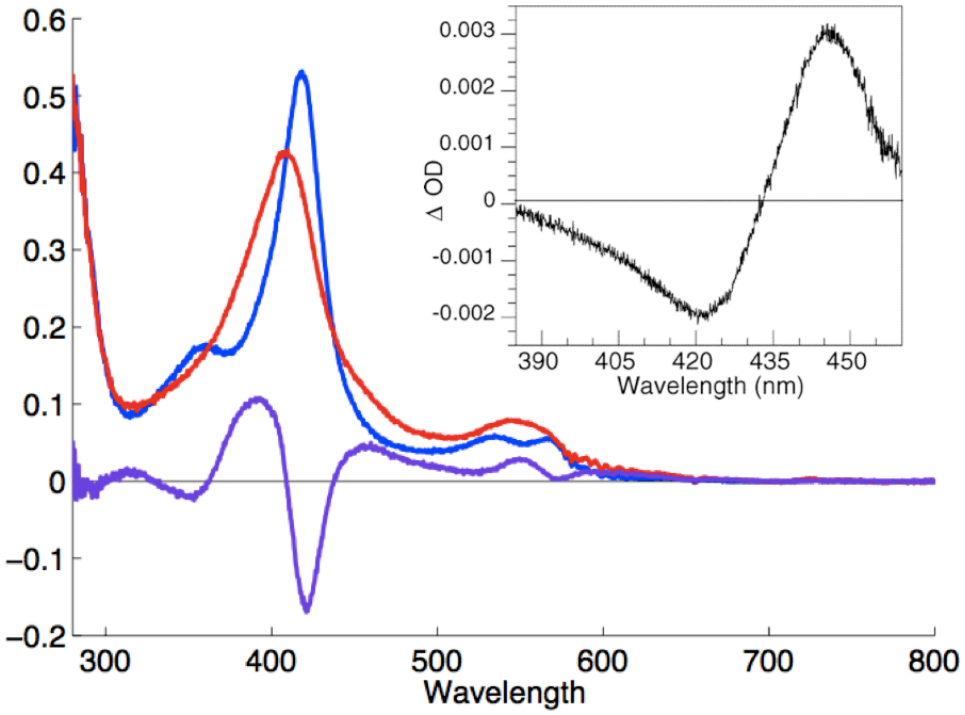

Figure 5.8. Spectra of ferric (blue) and ferrous (red) wild-type P450-BM3, and the ferrous – ferric difference spectrum (purple). **Inset**: Transient difference spectrum of photochemically reduced cytochrome $P450_{cam}$ by noncovalent Ru-wires.[23]

Fitting

Three kinetics phases are evident in the TA data. Thus, we performed a global least-squares fitting of the TA data recorded at 420 and 440 nm (and, for select mutants, 400, 410, 430 nm). Data were fit to a sum of three exponentials with amplitude coefficients $\rho_{1\text{-}3}$ and observed rate constants $\gamma_{1\text{-}3}$ (Equation 5.1). For fitting, see sample script in Appendix D. Similar to our analysis for photochemical heme *oxidation* described in Chapter 2, we fix the first observed rate constant as the quenched luminescence decay rate, as obtained from monoexponential fitting

of the luminescence decay at 630 nm. The remaining two rate constants are extracted from the global fitting, and are listed in **Table 5.2**.

$$y(n,t) = \rho_{n1}\exp(-\gamma_1 t) + \rho_{n2}\exp(-\gamma_2 t) + \rho_{n3}\exp(-\gamma_3 t) \quad (5.1)$$

Table 5.2. Rates of heme reduction extracted from global fitting of transient absorption data.

Enzyme	γ_1	γ_2	γ_3
Ru-K97C(W_{96})	1.6e7	3.6e4	1.1e2
Ru-K97C($_W H_{96}$)	1.6e7	6e4	1.9e2
Ru-D77C(H_{76})	1.9e7	5.7e4	1.4e2
Ru-D77C($_H W_{76}$)	1.9e7	8.1e4	1.3e2

The transient bleach at 420 nm and transient absorption at 440 nm observed on the microsecond timescale were assigned[23] as photochemical heme reduction (**Figure 5.8,** inset). Therefore, we assign the second rate constant as that of heme reduction. All four mutants exhibit very similar reduction rates, with maximum heme reduction complete at approximately 100 μs.

Interestingly, after normalizing by the magnitude of the $^*Ru^{II}$ excited state bleach (440 nm), the magnitudes of the transient features associated with heme reduction (e.g., absorption at 440 nm) differ greatly among the different mutants. In particular, both of the CYP119 mutants exhibit signals which are greater by a factor of 2-3 (**Figure 5.9**). Since we do not have extinction coefficients for the transiently reduced species, we cannot tell how much of this difference in signal is attributable to a difference in yield. However, it would be surprising if a difference in extinction coefficients could account for the entirety of this discrepancy.

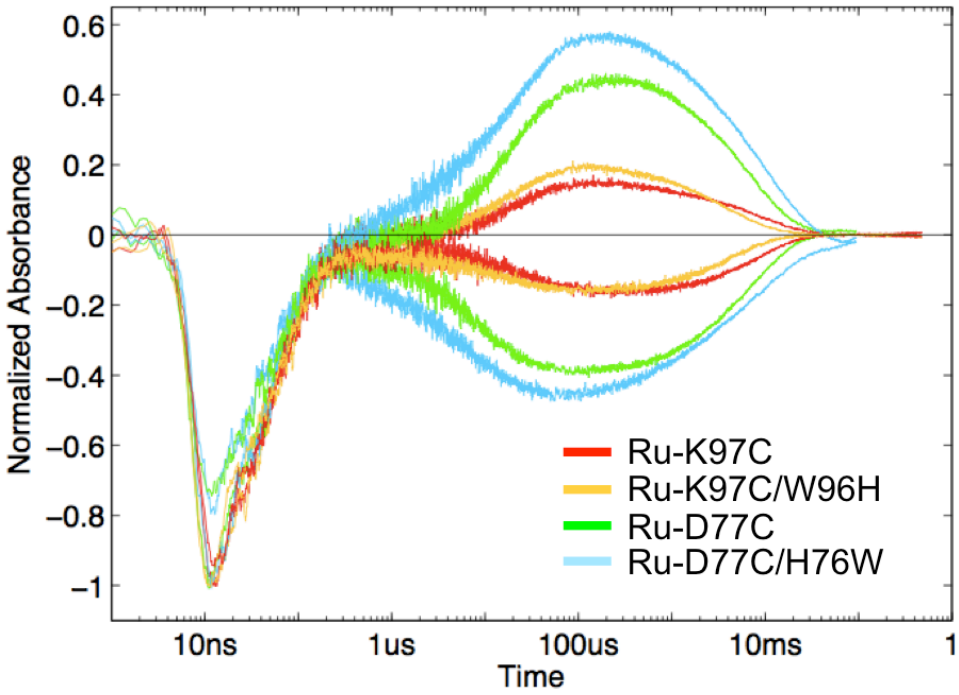

Figure 5.9. Normalized overlay of TA for the four Ru-P450 systems. 420 nm (ΔOD < 0 at 100 μs) and 440 nm (ΔOD > 0 at 100 μs), normalized to the intensity of the initial $^{*}Ru^{II}$ bleach (~10 ns) at 440 nm. Ru_{C97}-BM3(W_{96}) (red); Ru_{C97}-BM3($_{W}H_{96}$) (yellow), Ru_{C77}-CYP119(H_{76}) (green), Ru_{C77}-CYP119($_{H}W_{76}$) (blue).

All transient features decay to baseline within 100 ms; this return rate is extremely sensitive to small amounts of oxygen. In our proposed flash-quench scheme (**Figure 5.10**), re-oxidation of the ferrous center occurs via bimolecular recombination with oxidized *p*MeODMA. This recombination is expected to be a second order process; however, the disappearance of the transient features can be modeled as a first order process.

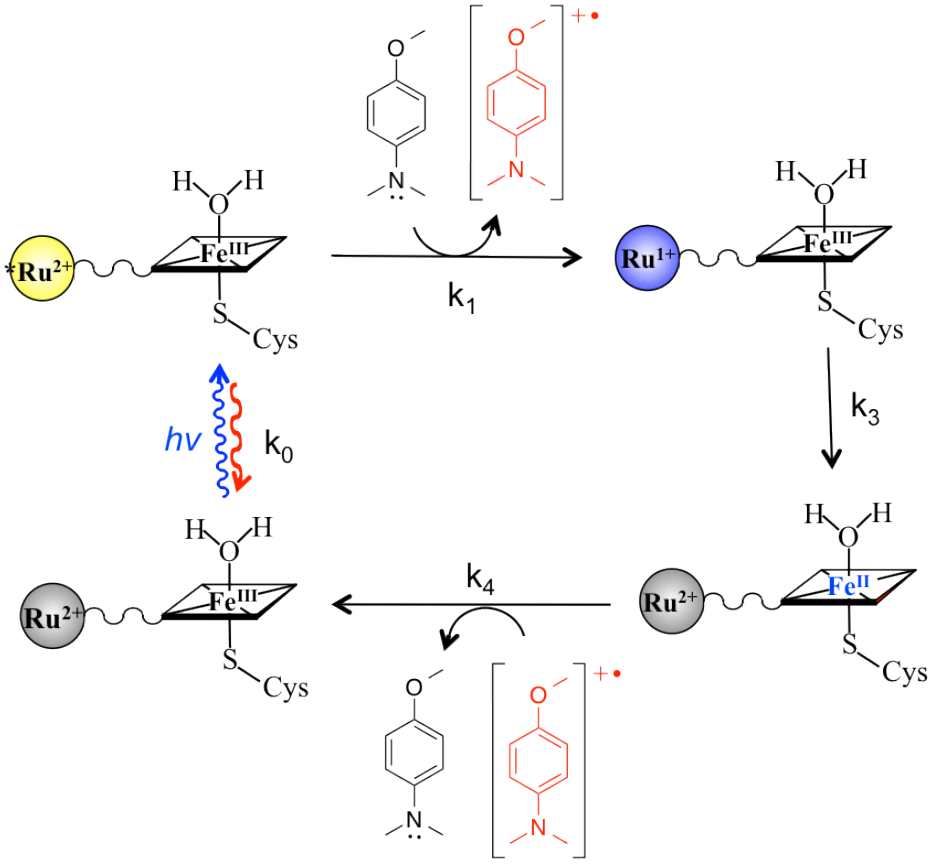

Figure 5.10. Flash-quench scheme for heme reduction.

Curiously, the transient absorbance at 510 nm, attributed to the oxidized *p*MeODMA radical, disappears much more quickly than reoxidation of the heme center (**Figure 5.6**). Accelerated quencher recovery was also observed upon oxidative quenching of Ru-P450 with methyl viologen (see Appendix C). This may be due to reaction of quencher radicals with trace amounts of oxygen. However, if this is the case, it remains unclear what reaction regenerates the resting state enzyme.

5.2.2. Reductive ET in the presence of CO

We anticipated that gas binding could be induced upon photochemical heme reduction. To that end, reductive flash-quench experiments were conducted under

an atmosphere of CO. However, the observed kinetics were irreproducible, and varied depending on the number of laser shots. Additionally, we observed the appearance of a shoulder at 450 nm in the sample absorbance spectrum, suggesting accumulation of Fe^{II}-CO. While we expected heme reduction and CO binding to be reversible, this observation suggests that newly generated Fe^{II}-CO persists on the order of minutes to hours. Somewhat unexpectedly, we also observed appearance of this shoulder at 450 nm even for pure protein samples in the *absence* of both photosensitizer and quencher (**Figure 5.11**).

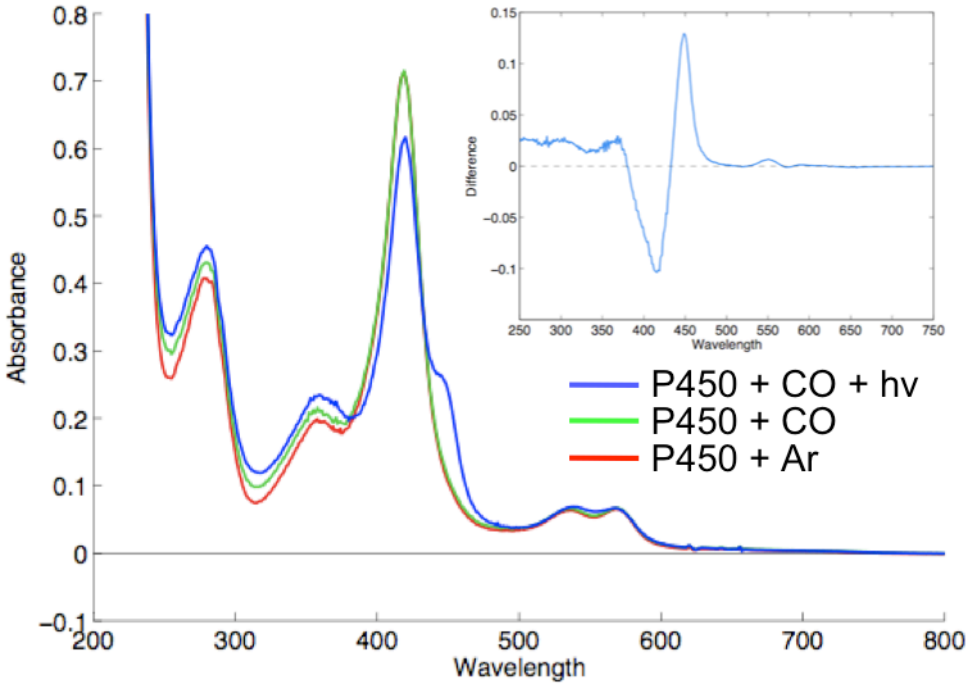

Figure 5.11. UV-visible absorbance spectra of Fe^{III}-P450 BM3 (double mutant: C62A/C156S, which contains no surface-exposed cysteines) under an atmosphere of argon (red) or an atmosphere of CO: before (green) and after (blue) excitation at 480 nm.

Samples that are not as rigorously deoxygenated do not show build-up of Fe^{II}–CO . This spontaneous reduction under irradiation of UV and visible light was observed for heme proteins, including P450.[25–27] It is possible that transient photo-reduced species are trapped by the CO. This process severely complicates the analysis of

transient data, as the Fe^{II}-CO concentration is in flux; and we cannot conclusively measure a rate for CO binding using this method of photo-triggered reduction.

This observation, along with other cited sources, brings into question the effectiveness of methods to photo-trigger heme reduction by excitation of NAD(P)H.[13] The organic reductant absorbs in the near UV, and overlaps extensively with the P450 absorption band at 360 nm. If P450 photo reduction and CO binding can be observed with excitation at 4 mJ/pulse of 480 nm, in the absence of any obvious chemical reductant, it is almost certain that 200 mJ/pulse radiation into the near-UV region of the P450 spectrum also would result in P450 reduction, albeit by a different mechanism than what was suggested by the authors.[12,13]

5.2.3. CO photolysis and rebinding

The rate of CO *re*binding can be measured following photolysis the Fe^{II}–CO bond of chemically-reduced ferrous–CO. In particular, we set out to examine the kinetics of CO rebinding for thermophilic CYP119 over a range of temperatures, in the presence and absence of substrate, and with a variety of laser pulse powers.

Samples for photolysis consist of WT CYP119 reduced with dithionite under an atmosphere of CO, in specialized, high-vacuum quartz cuvettes (see Appendix B). The P450 ferrous-CO species is characterized by a split-Soret spectrum with a Soret absorbance maximum at 448 nm. Photolysis of the Fe–CO bond produces a five-coordinate ferrous species, for which the Soret band is broader and significantly blue-shifted (**Figure 5.12**).

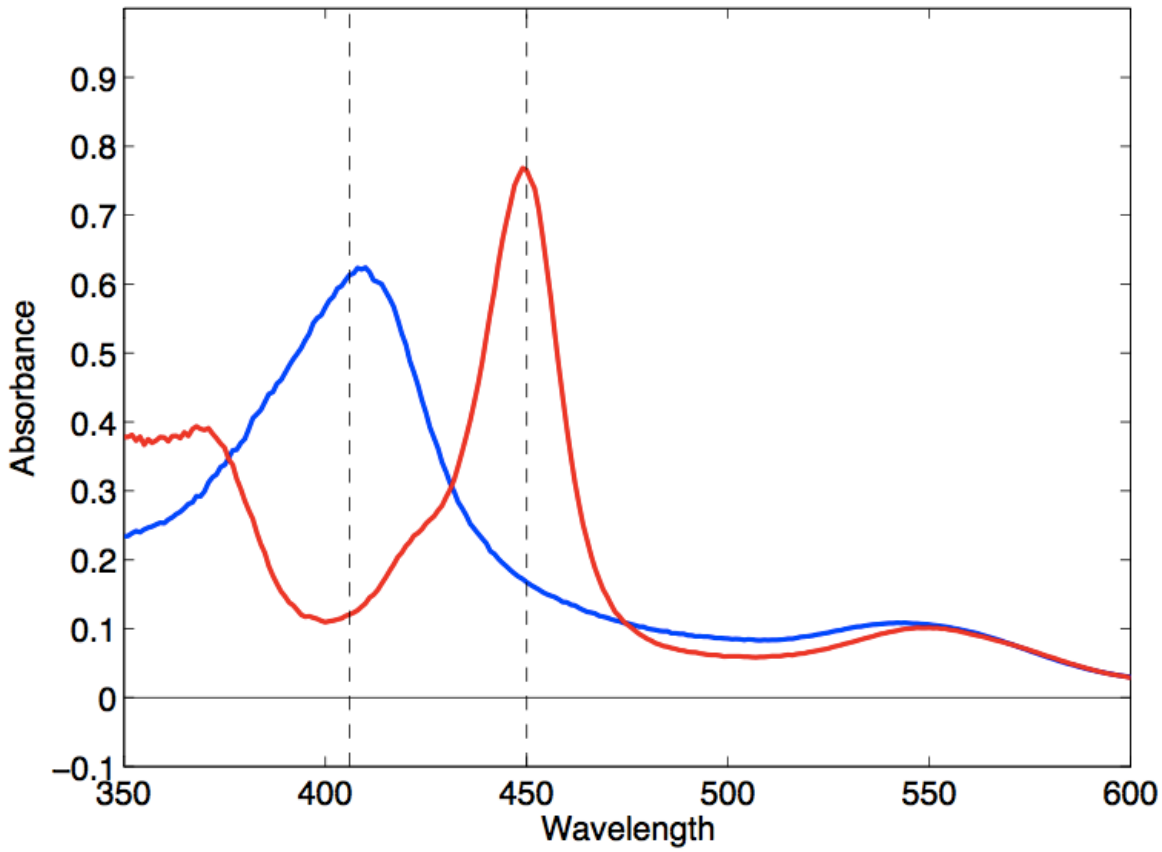

Figure 5.12. UV-visible absorbance spectra of five-coordinate, dithionite-reduced WT CYP119 (blue) and the corresponding six-coordinate ferrous CO species (red).

The multi-wavelength transient absorption spectra following excitation at 486 nm clearly show loss of the Fe^{II}–CO band at ~450 nm, and increase in absorption at ~400 nm (**Figure 5.13**). This transient spectrum is in excellent agreement with the Fe^{II}/Fe^{II}-CO difference spectrum (**Figure 5.13**, inset). By 4 ms, absorption has entirely returned to baseline, indicating full recovery of the starting, CO-bound ferrous species.

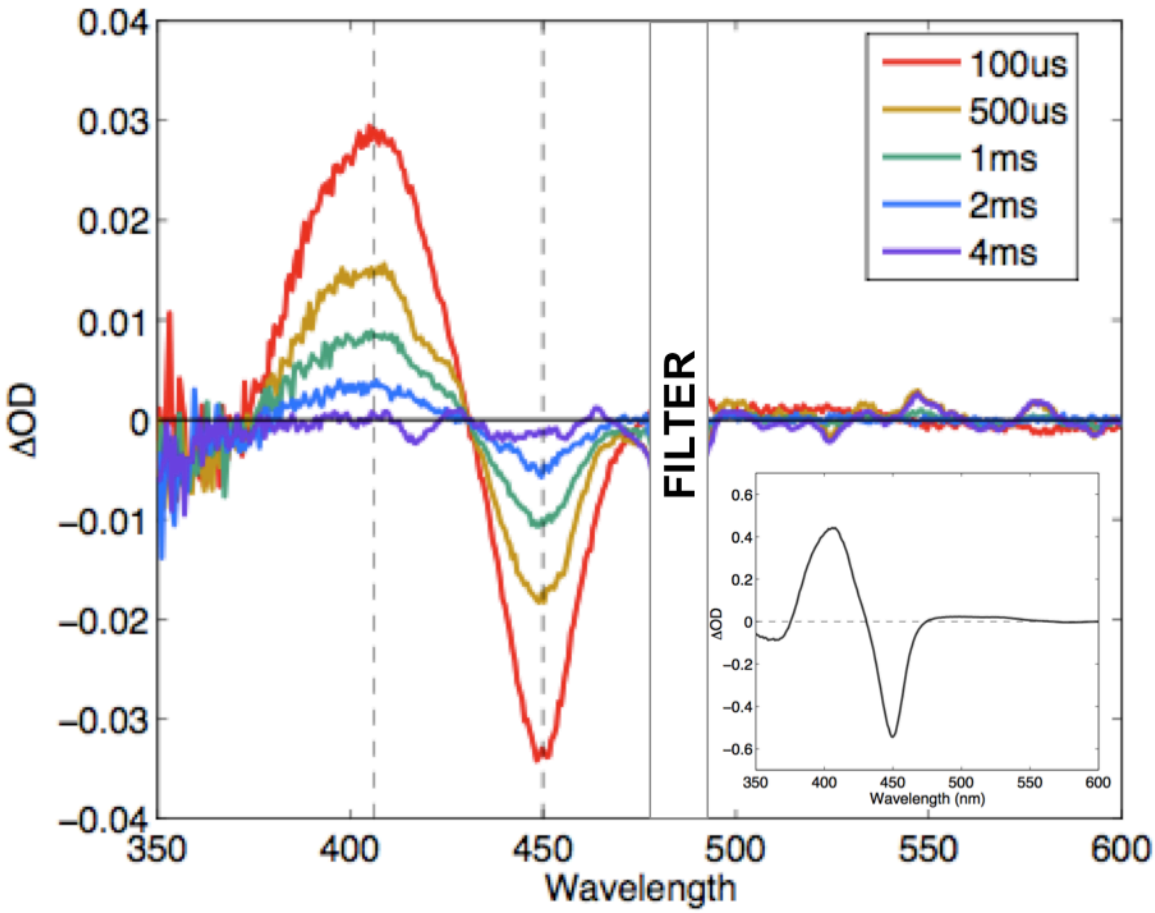

Figure 5.13. Transient difference spectra following flash-photolysis of WT CYP119 Fe^{II}-CO in 100 mM potassium phosphate buffer, pH 7.4, 20 °C. Excitation: 486 nm. A narrow notch filter blocks scattered laser light (and the probe light) 475-495 nm. Inset: Fe^{II}-Fe^{II}–CO difference spectrum.

As observed by single-wavelength transient absorption (**Figure 5.14**), two major kinetics components contribute to the recovery of the Fe^{II}-CO species. This behavior is commonly observed for CO rebinding in heme enzymes, including P450.[14–16] The fast rebinding phase is associated with geminate recombination, and typically occurs on the picosecond-to-nanosecond timescale. The slow rebinding phase is associated with CO that has escaped into solution and must diffuse back into the active site; this typically occurs on the millisecond timescale.

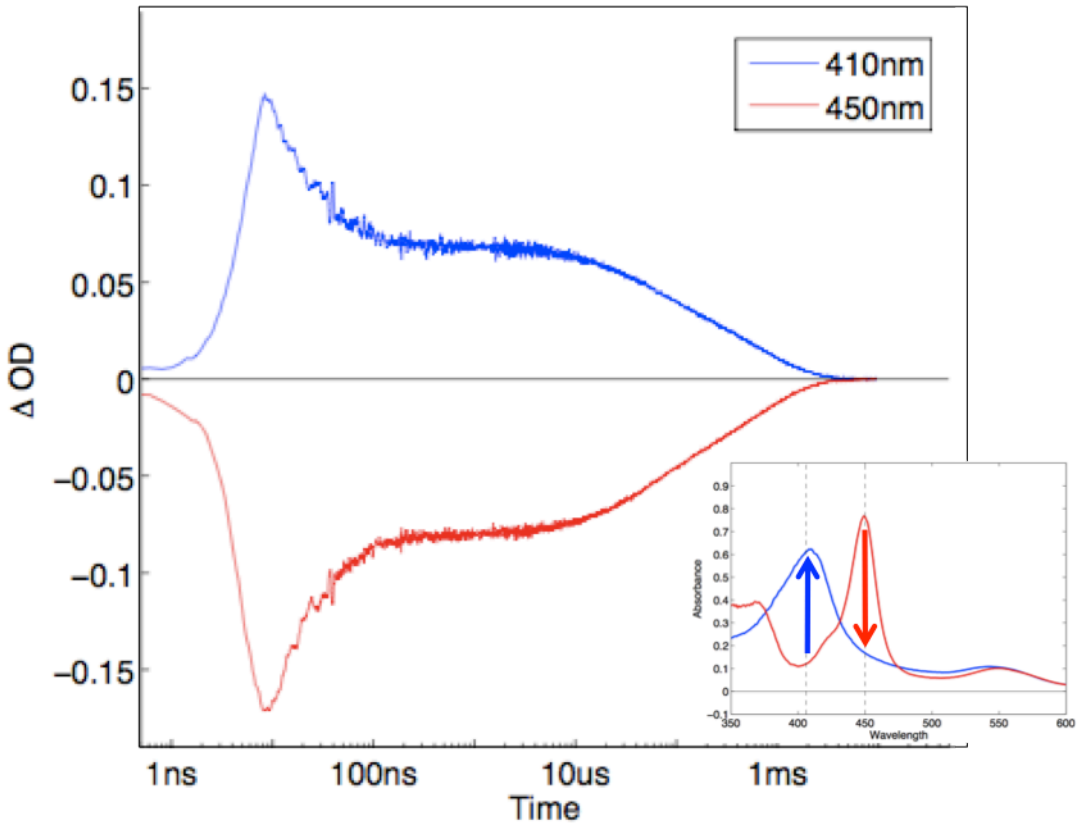

Figure 5.14. Single-wavelength TA following flash-photolysis of WT CYP119 Fe^{II}-CO in 100 mM potassium phosphate buffer, pH 7.4 buffer, 20 °C. Excitation: 460 nm. Single-wavelength transient absorption traces at 450 nm (red) and 410 nm (blue). **Inset**: Fe^{II}-$P450_{CYP119}$ (blue) and Fe^{II}-CO-$P450_{CYP119}$ (red).

In the presence of excess CO, one expects both geminate recombination and rebinding of escaped CO to obey first order and pseudo-first order kinetics (respectively). However, the single-wavelength TA data display complex kinetics behavior that cannot be fit to a sum of two exponentials. This also has been observed in flash photolysis of Fe^{II}-CO P450 BM3, and was attributed to multiple protein conformations with slow interconversion.[15] There is also evidence for multiple solution conformations of substrate-free CYP119, as examined by NMR spectroscopy and dynamics simulations.[28] Interestingly, these studies both suggest that P450 BM3 and CYP119 lock down into a dominant conformation in the presence of tightly binding substrates.

Power dependence and yield of CO escape

There is a nonlinear power dependence on the yield of CO escape, which appears to saturate around 10 mJ/pulse (**Figure 5.15**). If we assume that this saturation corresponds to 100% photolysis of the Fe–CO bond, then we can determine the yield of CO escape following photolysis.

Using the initial absorption spectrum of the Fe^{II}-CO sample (A_{450}=0.42), and the steady-state and transient difference spectra (**Figure 5.13**), we can determine the expected absorption at 100% conversion to five-coordinate Fe^{II}. The corresponding $\Delta OD(406)_{max}$ = 0.27; our maximum signal at power saturation is 0.13, just under 50% of the maximum signal. This is significantly lower than the previously reported CO escape yield of 64%.[17]

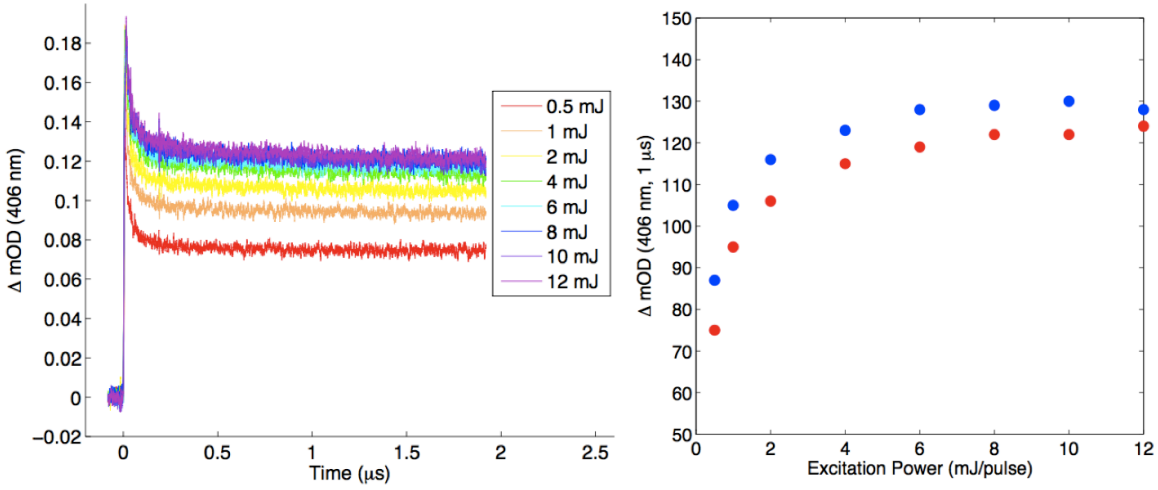

Figure 5.15. Power dependence of CO escape, 460 nm excitation, A_{450}=0.42. **Left**: Single-wavelength transient absorption at 406 nm. **Right**: Magnitude of CO escape for two samples, extracted from single wavelength TA data at 1 μs (red and blue dots; red corresponds to the figure on the right).

Temperature dependence (substrate-free)

CYP119 is an extremely thermostable protein, tolerating conditions of up to 90 °C or more. Therefore, we can examine a wide range of temperatures and determine its effect on the yields of CO escape and rates of rebinding. This temperature dependence is important for understanding the function of CYP119 under conditions that approximate those within its thermophilic parent organism, *Sulfolobus acidocaldarius*.

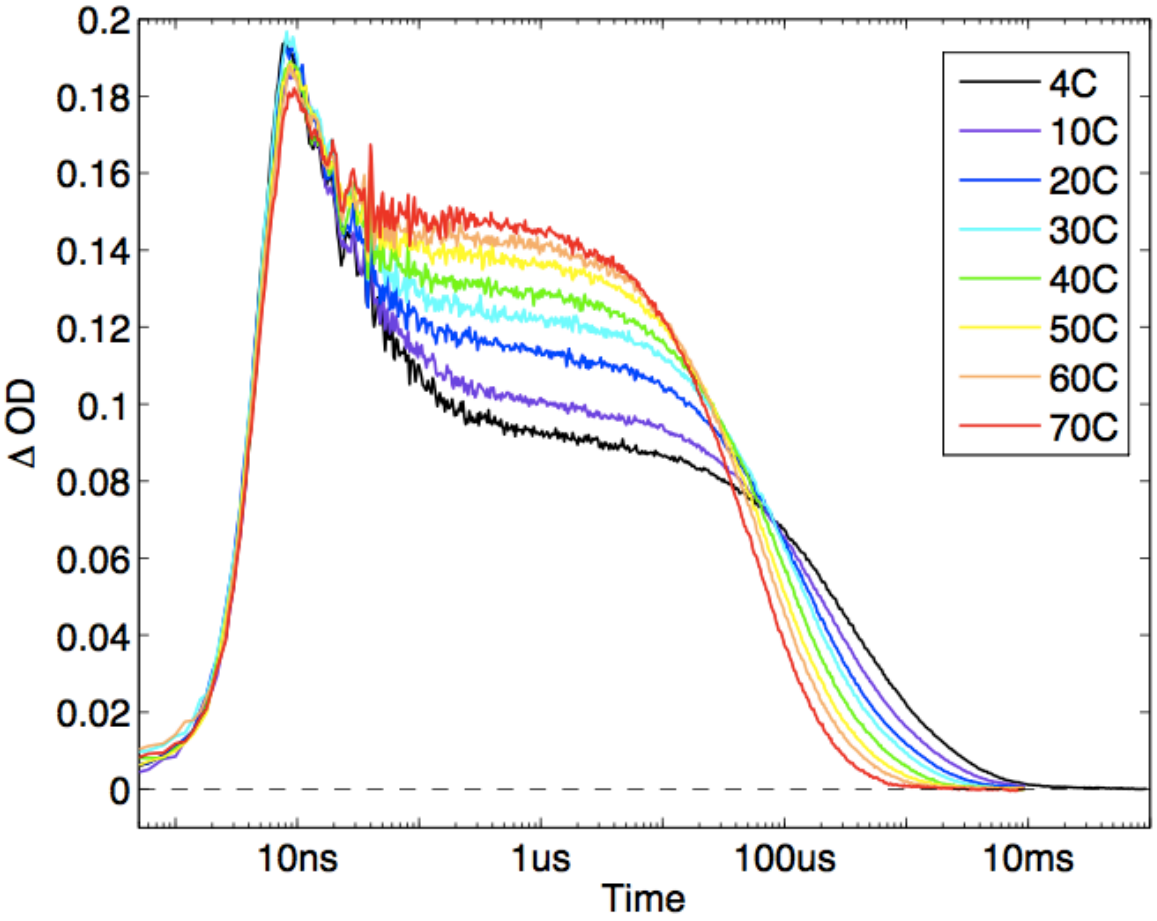

Figure 5.16. Temperature dependence of CO rebinding (no substrate). Abs(λ_{max} : 449 nm)=0.41, λ(excitation) = 460 nm, 2 mJ/pulse.

Reassuringly, temperature appears to have had little affect on the magnitude of the initial TA signal, and we assume that the total photolysis yield is constant. As

temperature increases, there is an increase in the yield of CO escape, as evidenced by the increased signal magnitude at ~ 1 μs. Additionally, the rate of CO rebinding increases with increased temperature.

Temperature dependence in the presence of laurate

We have examined the effect of bound fatty acid substrate on the rates of CO rebinding following photolysis. The native substrate of CYP119 is yet unknown, but this variant does tightly bind and hydroxylate various fatty acids *in vitro*.[29] Lauric acid (dodecanoic acid) is used here as a model substrate; the binding constant is reported to be 1.2 μM in CYP119.[29] Upon binding, the fatty acid partially displaces the axial water molecule, causing a shift to high-spin. This results in blue-shifting of the Soret band for laurate-bound CYP119 (**Figure 5.17**).

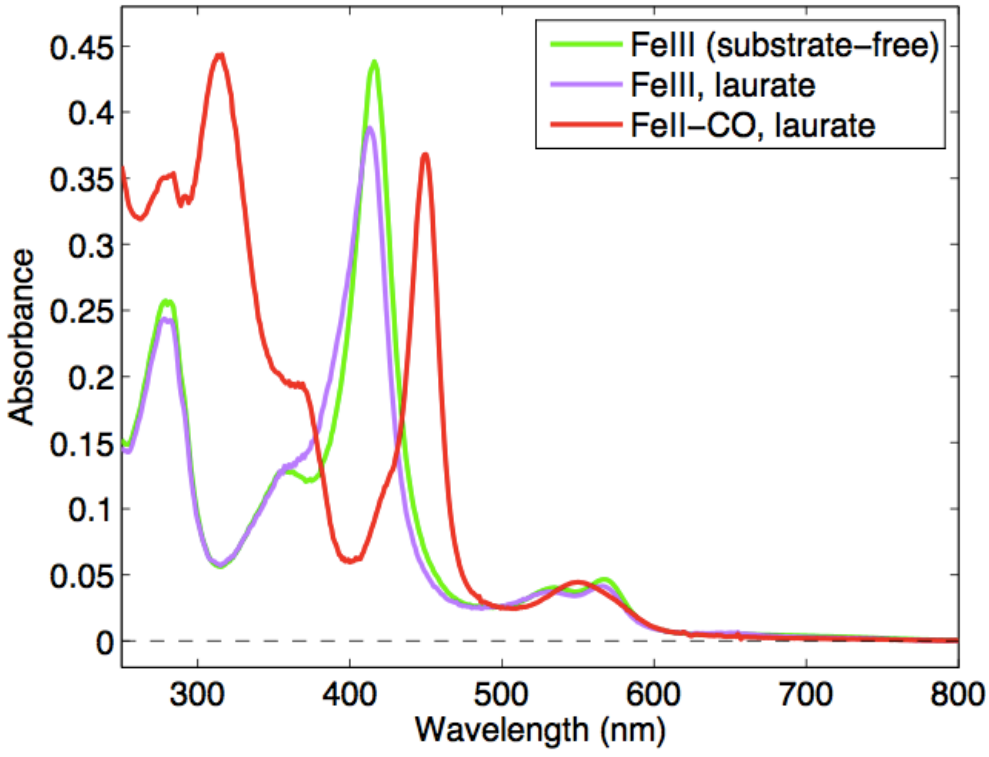

Figure 5.17. UV-visible absorption spectra of WT CYP119 with and without laurate. Green: Ferric, substrate-free. Purple: Ferric, 30 μM laurate. Red: Ferrous-CO, with 30 μM laurate. Samples have approximately equal concentrations.

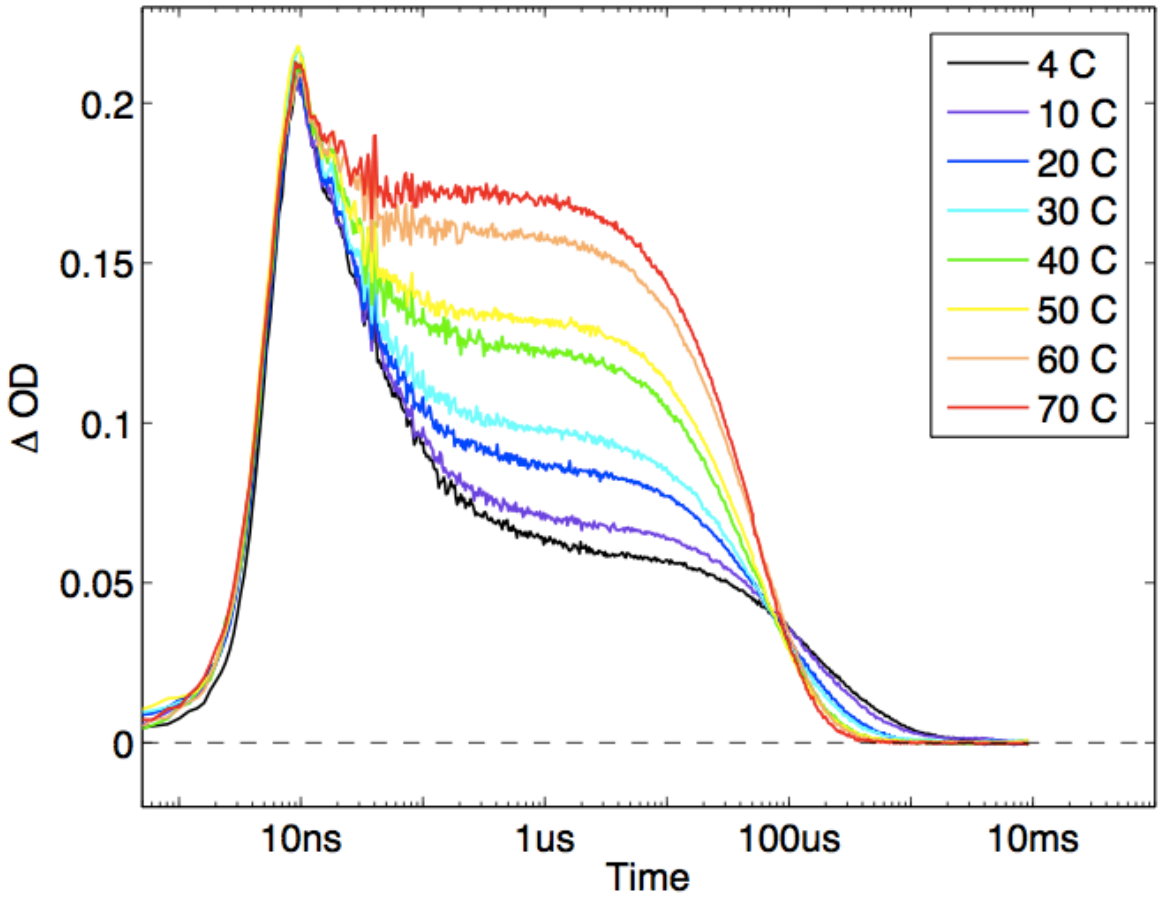

Figure 5.18. Temperature dependence of CO rebinding in the presence of 30 μM laurate. Abs(λ_{max}: 449 nm)=0.37, λ(excitation) = 460 nm, 2 mJ/pulse.

A similar temperature dependence of CO rebinding dynamics is observed in the presence of laurate; as temperature increases, there are increases in both the yield of CO escape and the rate of CO rebinding. In contrast to the substrate-free form, there appears to be a greater temperature dependence on yields of CO escape. At lower temperatures, there is a dramatic decrease in CO escape yield for the laurate-bound form (**Figure 5.19**, left); this discrepancy decreases as temperature increases.

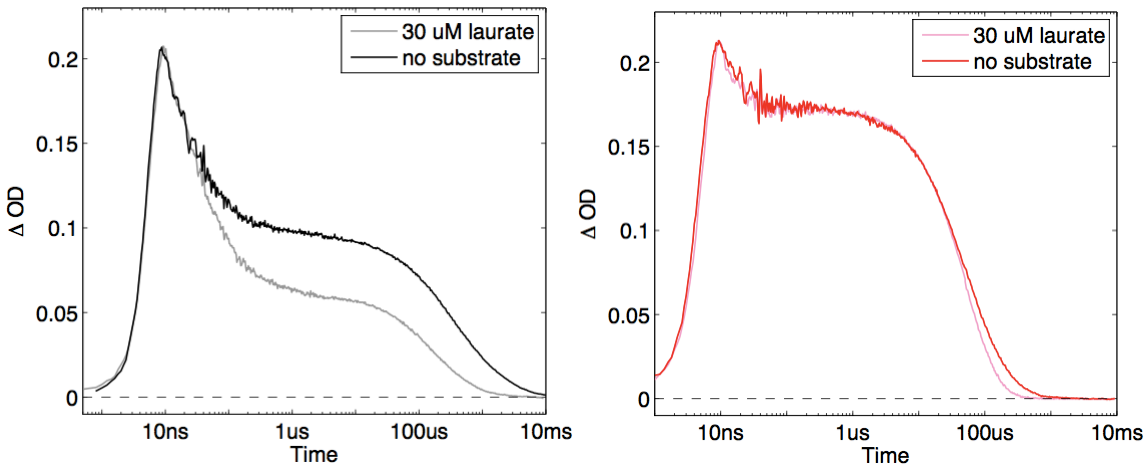

Figure 5.19. Comparison of laurate-free and laurate-bound CO rebinding kinetics (from Figure 5.16 and 5.17). Left: 20 °C. Dark blue, substrate free. Light blue, lauric acid bound; Right: 70 °C. Red, substrate free. Pink, substrate bound. Substrate-free traces have been multiplicatively scaled (x 1.06) to normalize the initial signal magnitude.

Picosecond transient absorption measurements

At high temperatures, geminate recombination appears to be complete within the instrument response in our nanosecond pulsed TA experiments; this is true in both substrate-free and substrate-bound forms. We have investigated the earlier timescales using picosecond-pulsed TA experiments (see appendix B for instrumentation). The signal-to-noise ratios are smaller for picosecond data, but the single-wavelength kinetics traces overlay nicely with nanosecond data (**Figure 5.20**, see Appendix C for a sample overlay).

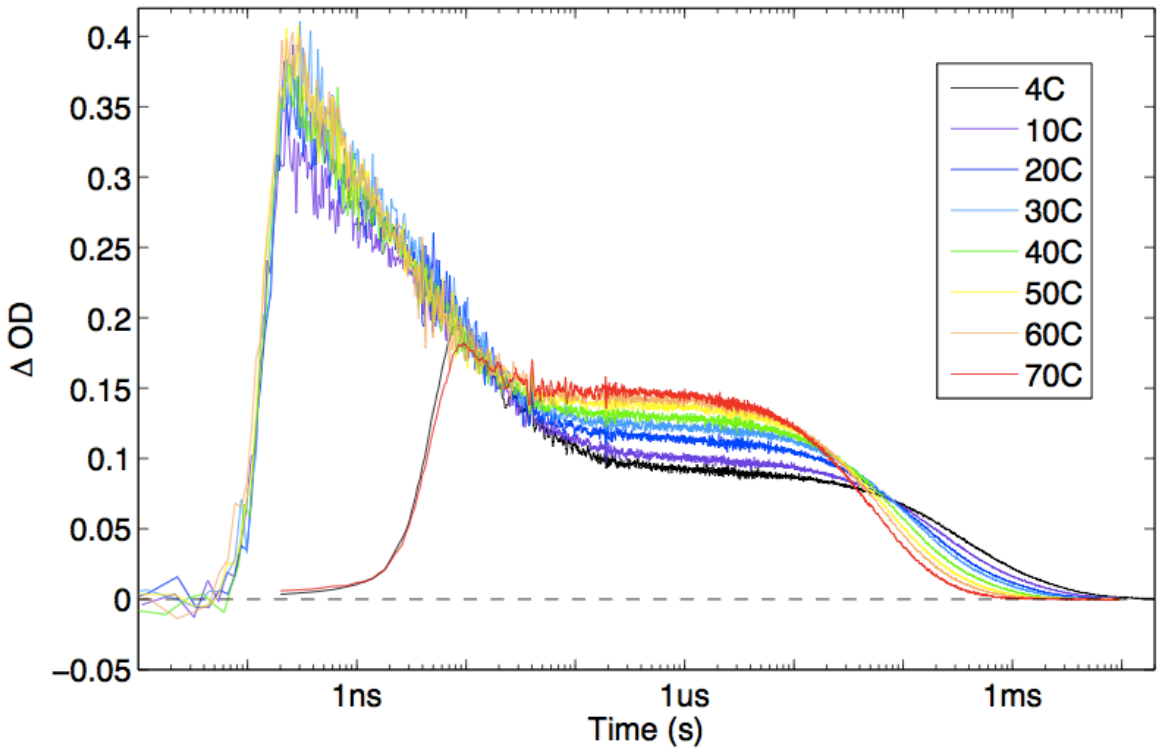

Figure 5.20. Picosecond-to-millisecond TA data for CO rebinding in substrate-free CYP119 at various temperatures. The picosecond data at 70 °C is significantly noiser and has been omitted.

Non-negative lease squares fitting

In order to more quantitatively assess the temperature dependence of CYP119 CO rebinding kinetics, we have subjected our transient absorption data to a nonnegative lease squares (nnls) fitting procedure. This is similar to the singular value decomposition analysis described in Chapter 2; single-wavelength transient absorption data are fit to a series of rate constants, and the fitting process provides amplitude coefficients corresponding to each rate constant. An additional constraint was added to limit the difference in amplitudes for adjacent rate constants (see Appendix D for matlab scripts).

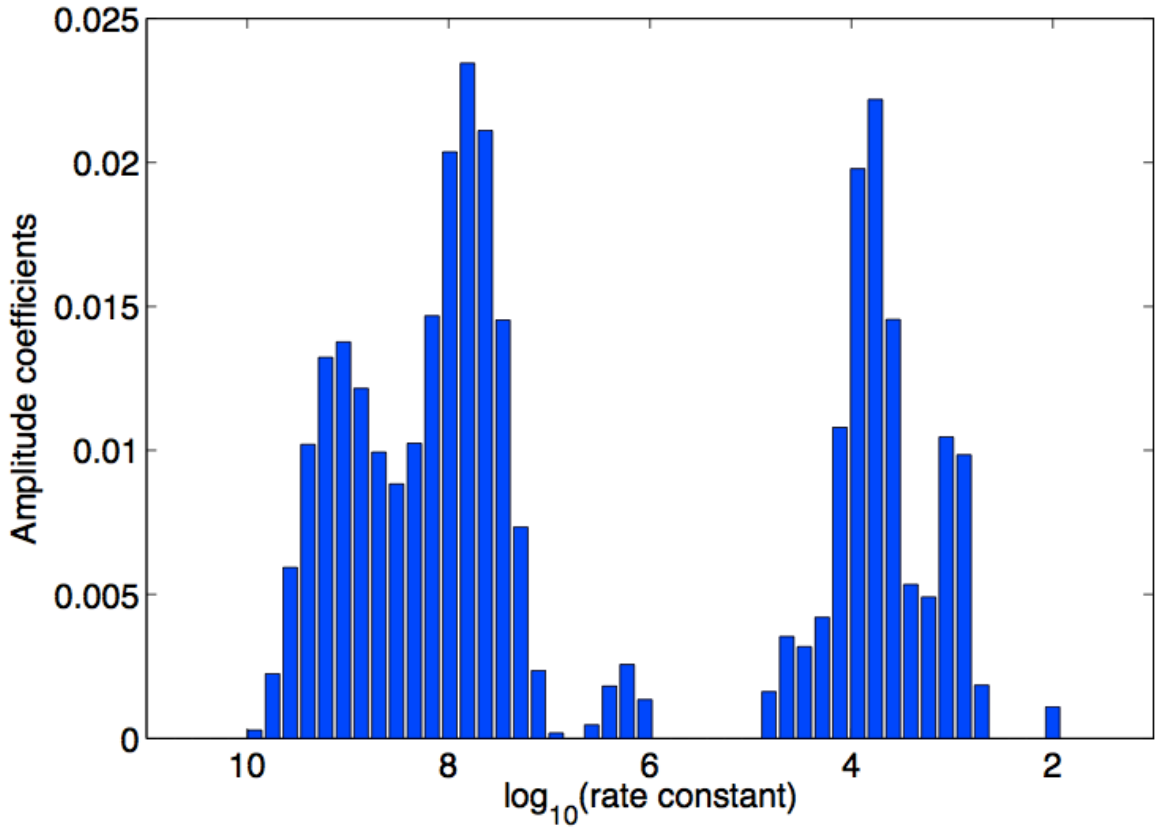

Figure 5.21. Amplitude coefficients derived from nonnegative least squares fitting of CYP119 CO rebinding kinetics. Conditions: 20 °C, no substrate. The lambda value associated with this fit is 1.297.

An example of the amplitude coefficients is shown in **Figure 5.21**; data from analysis of all temperatures can be found in Appendix C. As seen above, the rate constants from nnls fitting are divided into two major populations: the fast population (centered at $\log_{10}(k) \sim 8$) corresponds to geminate recombination, while the slow population (centered around $\log_{10}(k) \sim$ at.5) corresponds to rebinding of the escaped CO.

In order to further analyze the temperature dependence, we have integrated each population, and determined their first moment (mean), and second centered moment (variance).

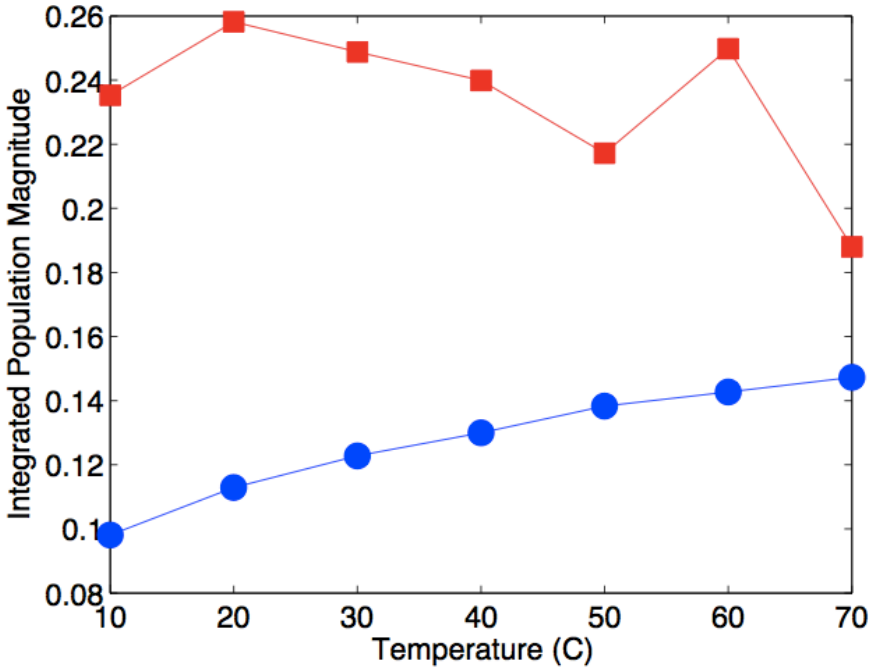

Figure 5.22. Integration of rate constant amplitudes at varying temperature (substrate free). Red: fast population corresponding to geminate recombination. Blue: slow population corresponding to rebinding of escaped CO.

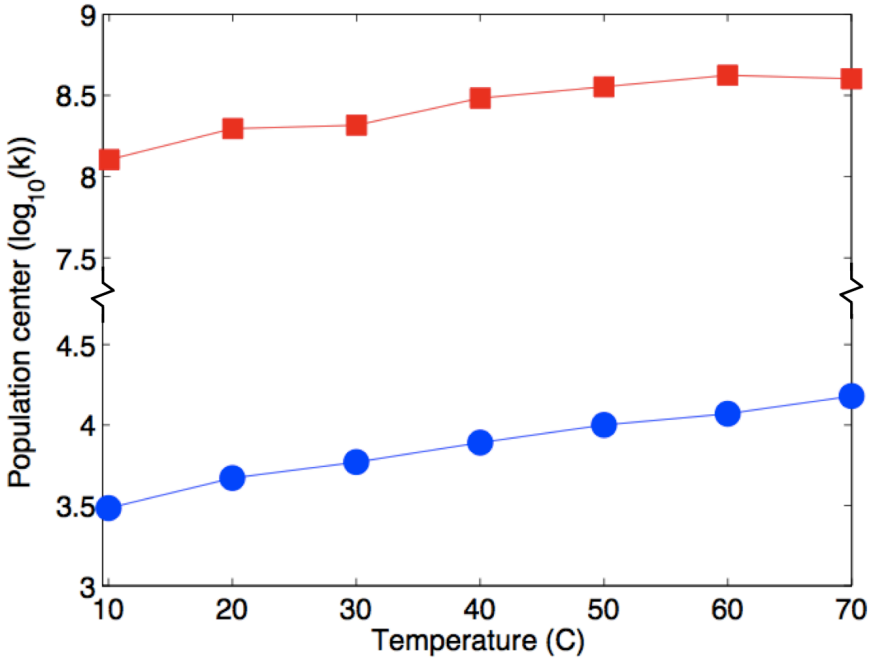

Figure 5.23. First moment of populations at varying temperature (substrate free). Note the break in the y-axis. Red: fast population corresponding to geminate recombination. Blue: slow population corresponding to rebinding of escaped CO.

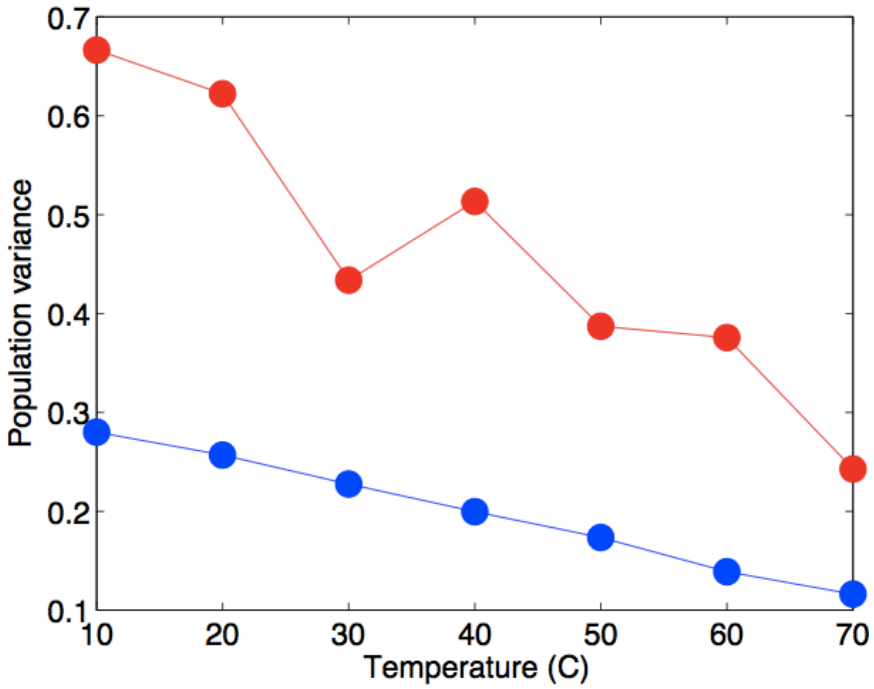

Figure 5.24. Second centered moment of populations at varying temperature (substrate free) Red: fast population corresponding to geminate recombination. Blue: slow population corresponding to rebinding of escaped CO.

As temperature increases, the integrated amplitude associated with the slow population increases in a nonlinear fashion (**Figure 5.22**); this corresponds to the increased yield of escaped CO. Due to increased noise associated with the fast component, it is not clear whether the integrated amplitude remains constant or decreases. The first moment of both the fast and slow components increase with temperature in a linear fashion (**Figure 5.23**). We use these population centers to do an Eyring analysis of the CO rebinding (vide infra). The second centered moment of both the fast and slow populations decreases as temperature increases (**Figure 5.24**). Intuitively, one might expect the opposite; as temperature increases, more conformations may become thermally accessed, leading to broadening of the population (and increase in the second centered moment). It is possible that there are multiple sub-populations within the fast and slow components, and that these

populations merge as temperature increases. Investigations into this possibility of subpopulations is ongoing in the Gray group.

The CO rebinding data for laurate-bound CYP119 are more preliminary, and have not been acquired on the picosecond timescale. Nevertheless, we have performed non-negative least squares fitting on the nanosecond-to-microsecond TA data (see **Figure 5.18** for TA data), and provide an initial comparison between rebinding of escaped CO in the presence and absence of laurate.

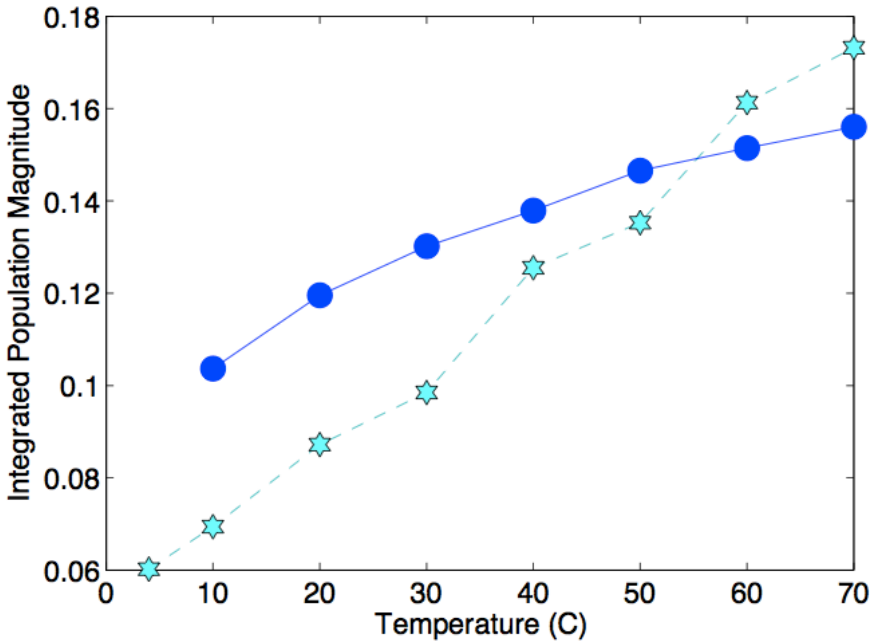

Figure 5.25. Comparison of amplitude integrations for the slow population in substrate-free and laurate-bound CYP119. Integrations of substrate-free data have been scaled multiplicatively by a factor of 1.06 to account for the slight difference in sample concentration and laser power.

As noted earlier, there is a larger temperature dependence for the yield of CO escape in the presence of laurate. It is plausible that the presence of substrate blocks some of the CO escape pathways, lowering the escape yield (and correspondingly lowering the integration of amplitudes). This is observed at lower temperature (< 50 °C). However, at high temperatures, the amplitudes associated

with CO escape appear to be *higher* in the presence of substrate. This intriguing phenomenon has not yet been explained, and deserves additional exploration.

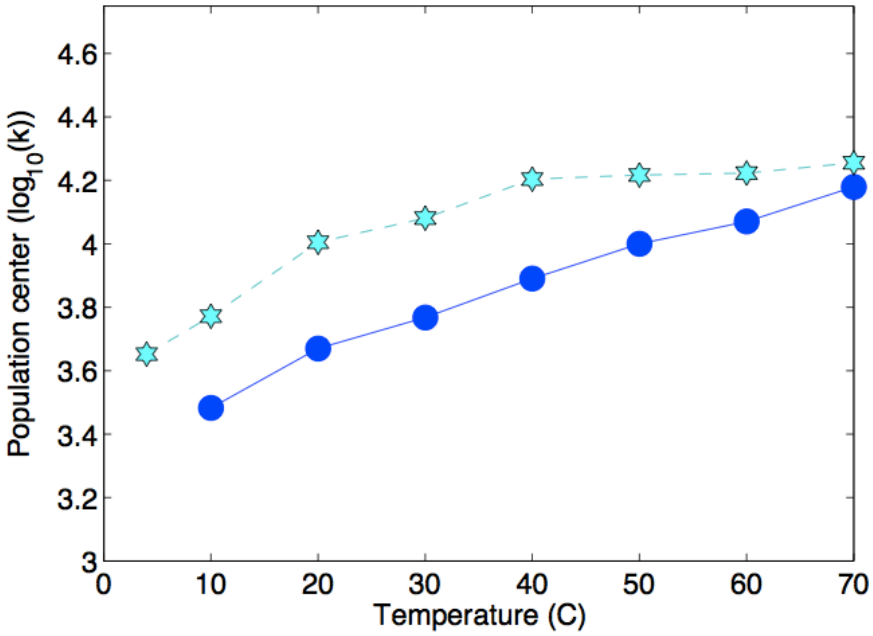

Figure 5.26. Comparison of slow population first moment in substrate-free and laurate-bound CYP119.

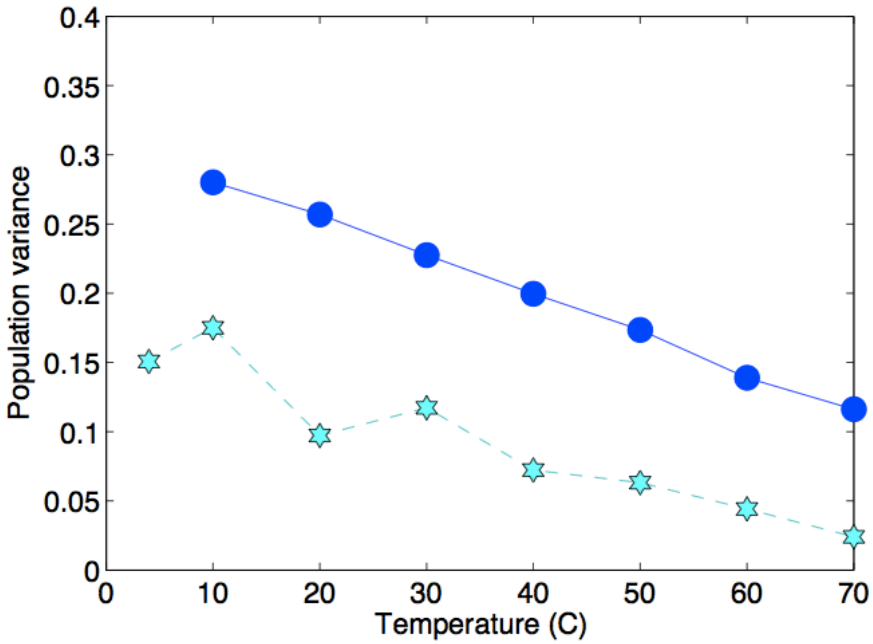

Figure 5.27. Comparison of slow population second centered moment (variance) in substrate-free and laurate-bound CYP119.

The rates of CO rebinding are faster in the presence of substrate; this is true throughout the temperature range, although the effect appears to diminish at higher temperatures. Interestingly, the opposite affect was observed for CO rebinding in P450 BM3[15] and P450cam.[30] This may indicate alternate pathways for CO re-entry among different P450 variants.

The final note in the substrate free/bound comparison is that the second moment (variance) in that the slow population distribution is significantly lower in the presence of substrate, over the entire temperature range. This is unsurprising, as tight binding to substrate causes significant structural shifts (see Chapter 1) and generates a single dominant conformation in solution.[28]

Eyring Analysis

We have performed an Eyring analysis on the kinetics of rebinding for escaped CO (slow population) in the substrate-free form. The data are consistent between samples, and are linear over the range of 10-70 °C (**Figure 5.28**). The extracted activation parameters are listed in **Table 5.3**. These thermodynamic parameters can be compared with those for other heme proteins, including $P450_{cam}$ [29] and myoglobin.[31]

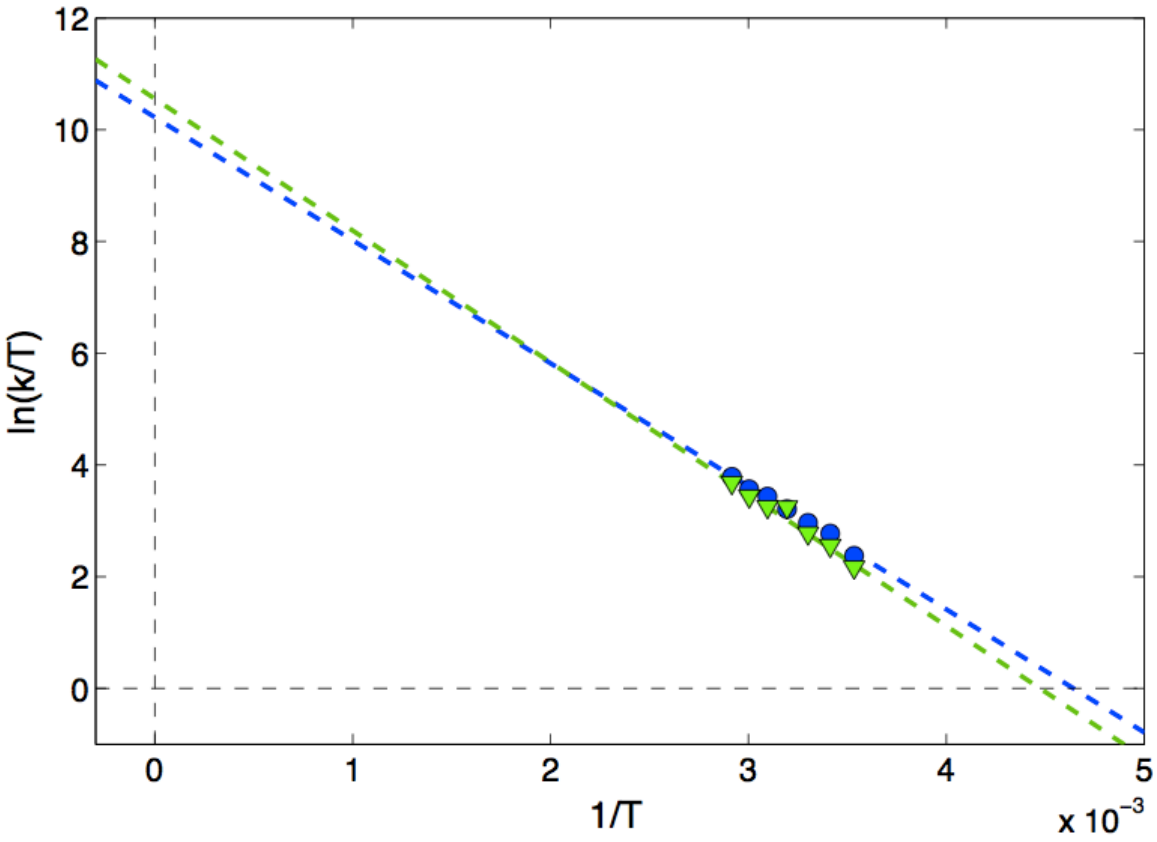

Figure 5.28. Eyring plot for rebinding of escaped CO in CYP119. The green triangles and blue circles represent two separate samples.

Table 5.3. Thermodynamic activation parameters for CO rebinding in CYP119 and various heme enzymes. a: this work. b: Reference 29. c: Reference 31.

Enzyme	$\Delta H^{\ddagger}$	$\Delta S^{\ddagger}$
	kcal/mol	cal/molK
CYP119[a] (substrate free)	4.5	-27
$P450_{cam}$[b] (substrate free)	14.2	21.6
$P450_{cam}$[b] (with camphor)	7.0	-12.4
Myoglobin[c]	4.1	-19.4

5.3. Discussion, Conclusions and Future works

We achieved rapid, photochemical reduction of the P450 active site of four Ru-P450 conjugates with a rate of 50,000 s^{-1}. By comparison, native ET between the fused reductase and heme domains in P450 BM3 occur at 220 s^{-1}.[32] Unlike the

photochemical oxidation discussed in Chapters 2 and 3, this reduction is not sensitive to intervening medium, and proceeds with rapid (microsecond) rates and good yields for all mutants examined. We also used photo-triggered methods to examine the kinetics of CO rebinding to wild type CYP119 following photolysis. We have identified key differences in the yields of CO escape, rates of rebinding, and population variance in the presence and absence of substrate, and have determined thermodynamic activation parameters for the substrate-free form. By selecting appropriate conditions of temperature, excitation wavelength, and buffer composition, we anticipate that these methods can be further refined to examine photochemical formation of ferric hydroperoxo species from chemically generated ferric superoxo, with the goal of observing the rearrangement to form CI.

5.4. Acknowledgments

The design, implementation, data collection, and analysis of picosecond TA were done with Dr. Kana Takematsu, and I am extremely grateful for her expertise, optimism, and perserverence. Discussions with Dr. Jay Winkler have been helpful for fitting, analyzing, and interpreting data. I also would like to thank Dr. Charlotte Whited for samples of the reductive quencher *p*MeODMA, and Professor Jeff Warren for assistance setting up the CO line.

5.5. Materials and Methods

Chemicals

Sodium dithionite (86%) was obtained from Fluka. Other buffer salts were obtained from J.T. Baker. *para*-methoxydimethylaniline (*p*MeODMA) used in these experiments was obtained courtesy of Dr. Charlotte Whited. Solutions were prepared using 18 MΩcm water unless otherwise noted.

Ru-P450 conjugates

The P450 mutants used for this study are: P450 BM3 C62A/C156S/K97C (C97-BM3(W)), C62A/C156S/K97C/W96H (C97-BM3($_{W}$H); CYP119 D77C (C77-CYP119(H)), D77C/H76W (C77-CYP119($_{H}$W)). The selection, mutagenesis, expression, and purification of cytochrome P450 mutants, as well as photosensitizer synthesis, conjugation, and purification, are described in Chapters 2 and 3.

Synthesis/purification of reductive quencher

The reductive quencher *para*-methoxydimethylaniline can be synthesized by previous published methods.[7] *p*MeODMA used in these experiments was obtained courtesy of Dr. Charlotte Whited, purified by sublimation and characterized by ^{1}H NMR.

*p*MeODMA is only sparingly soluble in water. 40 mM aqueous stock solutions were prepared by dissolving 5 mg in 200 μL of dimethylsulfoxide (DMSO), followed by dropwise (10 μL) addition of aqueous buffer (50 mM sodium borate, pH 8) to a total volume of 500 μL. Oxygenated solutions of *p*MeODMA change from clear to pinkish/purple in ambient light, with an absorbance increase at 550 nm. For that reason, fresh solutions were prepared immediately prior to use, and protected from light wherever possible.

Preparation of laser samples for flash-quench heme reduction

Laser samples were prepared in a high-vacuum four-sided quartz cuvette, sealed with a high-vacuum valve, and equipped with a small stir bar. Deoxygenation was achieved via gentle pump-backfill cycles with argon. For flash-quench in the presence of carbon monoxide, samples were subsequently pump-backfilled with

CO. Flash-quench samples consisted of approximately ~10 μM Ru-P450 (Ru_{C97}-BM3(W), Ru_{C97}-BM3($_{W}$H), Ru_{C77}-CYP119(H) or Ru_{C77}-CYP119($_{H}$W)) with 10 mM *p*MeODMA in buffered solution: 50 mM sodium borate buffer, pH 8. Samples were excited with 8 ns laser pulses at 480 nm. Luminescence decays were monitored at 630 nm. Single wavelength transient absorption (TA) kinetics were monitored every 10 nm from 390-440 nm, averaging ~500 shots per wavelength. Data from five separate timescales (2 μs, 40 μs, 400 μs, 10 ms, and 500 ms) were collected, log-compressed, and spliced together to produce full kinetics traces. See Appendix D for log-compression and splicing scripts in Matlab.

Preparation of samples for Fe^{II}-CO photolysis/rebinding

Flash-photolysis samples were prepared in a specialized high-vacuum 4-sided quartz cuvette containing an attached 10 mL bulb compartment and a 24/40 adaptor; each compartment could be sealed separately by a high-vacuum valve (Kontes) (see diagram in Appendix B). Approximately 1.5 mL of ferric wild-type CYP119 (3-10 μM for ns-pulsed experiments, 30-60 μM for ps-pulsed experiments) in 100 mM potassium phosophate buffer, pH 7.4, was placed in the cuvette portion. A few grains of sodium dithionite were added to the bulb compartment, and the entire apparatus was degassed by gentle pump-backfill cycles with argon. The cuvette was then subjected to gentle pump-backfill cycles with carbon monoxide to obtain a headspace of CO. While sealed from the atmosphere, the ferric protein solution was mixed with sodium dithionite in the bulb, and then returned to the cuvette portion.

For nanosecond-to-millisecond TA experiments, samples were excited with 8 ns laser pulses at either 460 nm (single wavelength TA) or 486 nm (multi-wavelength TA). For single-wavelength transient absorption measurements, a narrow

bandpass filter (centered at 406 nm, Appendix C) was used to block the majority of the white probe light.

For picosecond-to-nanosecond TA experiments, samples were excited with 30 ps laser pulses at 532 nm with 0.5-1 mJ/pulse, and a 405 nm laser diode was used as probe light.

5.6. References

(1) Noble, M. A.; Miles, C. S.; Chapman, S. K.; Lysek, D. A.; Mackay, A. C.; Reid, G. A.; Hanzlik, R. P.; Munro, A. W. Roles of Key Active-Site Residues in Flavocytochrome P450 BM3. *Biochem. J.* **1999**, *339*, 371–379.

(2) Rittle, J.; Green, M. T. Cytochrome P450 Compound I: Capture, Characterization, and C-H Bond Activation Kinetics. *Science* **2010**, *330*, 933–937.

(3) Davydov, R.; Makris, T. M.; Kofman, V.; Werst, D. E.; Sligar, S. G.; Hoffman, B. M. Hydroxylation of Camphor by Reduced Oxy-Cytochrome P450cam: Mechanistic Implications of EPR and ENDOR Studies of Catalytic Intermediates in Native and Mutant Enzymes. *J. Am. Chem. Soc.* **2001**, *123*, 1403–1415.

(4) Sutin, N.; Creutz, C. Properties and Reactivities of the Luminescent Excited States of Polypyridine Complexes of Ruthenium(II) and Osmium(II). In *Inorganic and Organometallic Photochemistry*; Advances in Chemistry; American Chemical Society: Washington, DC, 1978; Vol. 1.

(5) Creutz, C.; Chou, M.; Netzel, T. L.; Okumura, M.; Sutin, N. Lifetimes, Spectra, and Quenching of the Excited States of Polypyridine Complexes of Iron(II), Ruthenium(II), and Osmium(II). *J. Am. Chem. Soc.* **1980**, *102*, 1309–1319.

(6) Coelho, P. S.; Wang, Z. J.; Ener, M. E.; Baril, S. A.; Kannan, A.; Arnold, F. H.; Brustad, E. M. A Serine-Substituted P450 Catalyzes Highly Efficient Carbene Transfer to Olefins in Vivo. *Nat. Chem. Biol.* **2013**, *9*, 485–487.

(7) Mines, G. A.; Bjerrum, M. J.; Hill, M. G.; Casimiro, D. R.; Chang, I.-J.; Winkler, J. R.; Gray, H. B. Rates of Heme Oxidation and Reduction in Ru(His33)cytochrome c at Very High Driving Forces. *J. Am. Chem. Soc.* **1996**, *118*, 1961–1965.

(8) Sevrioukova, I. F.; Immoos, C. E.; Poulos, T. L.; Farmer, P. J. Electron Transfer in the Ruthenated Heme Domain of Cytochrome P450BM-3. *Isr. J. Chem.* **2000**, *40*, 47–53.

(9) Loida, P. J.; Sligar, S. G. Molecular Recognition in Cytochrome-P-450 - Mechanism for the Control of Uncoupling Reactions. *Biochemistry* **1993**, *32*, 11530–11538.

(10) Martinis, S. A.; Blanke, S. R.; Hager, L. P.; Sligar, S. G.; Hoa, G. H. B.; Rux, J. J.; Dawson, J. H. Probing the Heme Iron Coordination Structure of Pressure-Induced Cytochrome P420(cam). *Biochemistry* **1996**, *35*, 14530–14536.

(11) Perera, R.; Sono, M.; Sigman, J. A.; Pfister, T. D.; Lu, Y.; Dawson, J. H. Neutral Thiol as a Proximal Ligand to Ferrous Heme Iron: Implications for

Heme Proteins That Lose Cysteine Thiolate Ligation on Reduction. *Proc. Natl. Acad. Sci.* **2003**, *100*, 3641–3646.

(12) Dunford, A. J.; McLean, K. J.; Sabri, M.; Seward, H. E.; Heyes, D. J.; Scrutton, N. S.; Munro, A. W. Rapid P450 Heme Iron Reduction by Laser Photoexcitation of Mycobacterium Tuberculosis CYP121 and CYP51B1 - Analysis of CO Complexation Reactions and Reversibility of the P450/P420 Equilibrium. *J. Biol. Chem.* **2007**, *282*, 24816–24824.

(13) Girvan, H. M.; Heyes, D. J.; Scrutton, N. S.; Munro, A. W. Laser Photoexcitation of NAD(P)H Induces Reduction of P450 BM3 Heme Domain on the Microsecond Timescale. *J. Am. Chem. Soc.* **2007**, *129*, 6647–6653.

(14) Lange, R.; Heiberlanger, I.; Bonfils, C.; Fabre, I.; Negishi, M.; Balny, C. Activation Volume and Energetic Properties of the Binding of CO to Hemoproteins. *Biophys. J.* **1994**, *66*, 89–98.

(15) McLean, M. A.; Yeom, H.; Sligar, S. G. Carbon Monoxide Binding to Cytochrome P450(BM-3): Evidence for a Substrate Dependent Conformational Change. *Biochimie* **1996**, *78*, 700–705.

(16) Rupenyan, A.; Commandeur, J.; Groot, M. L. CO Photodissociation Dynamics in Cytochrome P450BM3 Studied by Subpicosecond Visible and Mid-Infrared Spectroscopy. *Biochemistry* **2009**, *48*, 6104–6110.

(17) McLean, M. A.; Maves, S. A.; Weiss, K. E.; Krepich, S.; Sligar, S. G. Characterization of a Cytochrome P450 from the Acidothermophilic Archaea Sulfolobus Solfataricus. *Biochem. Biophys. Res. Commun.* **1998**, *252*, 166–172.

(18) Perera, R.; Sono, M.; Raner, G. M.; Dawson, J. H. Subzero-Temperature Stabilization and Spectroscopic Characterization of Homogenous Oxyferrous Complexes of the Cytochrome P450BM3 (CYP102) Oxygenase Domain and Holoenzyme. *Biochem. Biophys. Res. Commun.* **2005**, *338*, 365–371.

(19) Castellano, F. N.; Dattelbaum, J. D.; Lakowicz, J. R. Long-Lifetime Ru(II) Complexes as Labeling Reagents for Sulfhydryl Groups. *Anal. Biochem.* **1998**, *255*, 165–170.

(20) Sassoon, R. E.; Gershuni, S.; Rabani, J. Photochemical Generation and Consequent Stabilization of Electron-Transfer Products on Separate like-Charged Polyelectrolytes. *J. Phys. Chem.* **1992**, *96*, 4692–4698.

(21) Mines, G. A. Cytochrome c: Folding Triggered by Electron Transfer. Rates of Heme Oxidation and Reduction at High Driving Forces, California Institute of Technology: Pasadena, California, 1997.

(22) Whited, C. A.; Belliston-Bittner, W.; Dunn, A. R.; Winkler, J. R.; Gray, H. B. Nanosecond Photoreduction of Inducible Nitric Oxide Synthase by a Ru-

Diimine Electron Tunneling Wire Bound Distant from the Active Site. *J. Inorg. Biochem.* **2009**, *103*, 906–911.

(23) Dunn, A.; Dmochowski, I.; Winkler, J.; Gray, H. Nanosecond Photoreduction of Cytochrome P450cam by Channel-Specific Ru-Diimine Electron Tunneling Wires. *J. Am. Chem. Soc.* **2003**, *125*, 12450–12456.

(24) Denisov, I. G.; Makris, T. M.; Sligar, S. G. Cryoradiolysis for the Study of P450 Reaction Intermediates. *Methods Enzymol.* **2002**, *357*, 103–115.

(25) Pierre, J.; Bazin, M.; Debey, P.; Santus, R. One-Electron Photo-Reduction of Bacterial Cytochrome P-450 by Ultraviolet-Light. 1. Steady-State Irradiations. *Eur. J. Biochem.* **1982**, *124*, 533–537.

(26) Bazin, M.; Pierre, J.; Debey, P.; Santus, R. One-Electron Photoreduction of Bacterial Cytochrome P-450 by Ultraviolet Light. II. A Study Using Laser Flash Photolysis of the Dynamics of the Reduction of Bacterial Cytochrome P-450 in the Presence of Carbon Monoxide. The Role of the PRotein Conformation. *Eur. J. Biochem.* **1982**, *124*, 539–544.

(27) Gu, Y.; Li, P.; Sage, T.; Champion, P. M. Photoreduction of Heme-Proteins - Spectroscopic Studies and Cross-Section Measurements. *J. Am. Chem. Soc.* **1993**, *115*, 4993–5004.

(28) Lampe, J., N.; Brandman, R.; Sivaramakrishnan, S.; de Montellano, P. R. O. Two-Dimensional NMR and All-Atom Molecular Dynamics of Cytochrome P450 CYP119 Reveal Hidden Conformational Substates. *J. Biol. Chem.* **2010**, *285*, 9594–9603.

(29) Koo, L. S.; Immoos, C. E.; Cohen, M. S.; Farmer, P. J.; Ortiz de Montellano, P. R. Enhanced Electron Transfer and Lauric Acid Hydroxylation by Site-Directed Mutagenesis of CYP119. *J. Am. Chem. Soc.* **2002**, *124*, 5684–5691.

(30) Tian, W. D.; Wells, A. V.; Champion, P. M.; Di Primo, C.; Gerber, N.; Sligar, S. G. Measurements of CO Geminate Recombination in Cytochromes P450 and P420. *J. Biol. Chem.* **1995**, *270*, 8672–8679.

(31) Hasinoff, B. B. Kinetic Activation Volumes of the Binding of Oxygen and Carbon Monoxide to Hemoglobin and Myoglobin Studied on a High-Pressure Laser Flash Photolysis Apparatus. *Biochemistry* **1974**, *13*, 3111–3117.

(32) Munro, A. W.; Daff, S.; Coggins, J. R.; Lindsay, J. G.; Chapman, S. K. Probing Electron Transfer in Flavocytochrome P-450 BM3 and Its Component Domains. *Eur. J. Biochem.* **1996**, *239*, 403–409.